

1 **Using top-down modulation to optimally balance shared versus separated task representations**

2

3 *Authors: Pieter Verbeke¹ & Tom Verguts¹*

4 *Affiliations:* ¹Department of experimental psychology; Ghent University

5 ORCID IDs: Pieter Verbeke: 0000-0003-2919-1528

6 Tom Verguts: 0000-0002-7783-4754

7 Corresponding author email: pjverbek.verbeke@ugent.be

8

9 Keywords: Cognitive control, modulation, neural representations, generalization

10

11 **Declarations**

12

13 **Funding :** PV was supported by grant 1102519N from Research Foundation Flanders. TV was

14 supported by grant BOF17/GOA/004 from the Ghent University Research Council.

15

16 **Acknowledgements:** We thank Sebastian Musslick, Senne Braem, Cristian Buc Calderon and Pieter

17 Huycke for valuable comments on this work. We also thank Michael J. Frank and his lab members for

18 interesting input.

19

20 **Data availability statement:** Code to simulate the model and analyze the resulting data is provided

21 in our GitHub repository: https://github.com/CogComNeuroSci/PieterV_public/tree/master/Gating

Abstract

22 Human adaptive behavior requires continually learning and performing a wide variety of tasks, often
23 with very little practice. To accomplish this, it is crucial to separate neural representations of different
24 tasks in order to avoid interference. At the same time, sharing neural representations supports
25 generalization and allows faster learning. Therefore, a crucial challenge is to find an optimal balance
26 between shared versus separated representations. Typically, models of human cognition employ top-
27 down modulatory signals to separate task representations, but there exist surprisingly little systematic
28 computational investigations of how such modulation is best implemented. We identify and
29 systematically evaluate two crucial features of modulatory signals. First, top-down input can be
30 processed in an additive or multiplicative manner. Second, the modulatory signals can be adaptive
31 (learned) or non-adaptive (random). We cross these two features, resulting in four modulation networks
32 which are tested on a variety of input datasets and tasks with different degrees of stimulus-action
33 mapping overlap. The multiplicative adaptive modulation network outperforms all other networks in
34 terms of accuracy. Moreover, this network develops hidden units that optimally share representations
35 between tasks. Specifically, different than the binary approach of currently popular latent state models,
36 it exploits partial overlap between tasks.

37

1. Introduction

38

39

40

41

42

43

44

45

46

47

Humans and other rational agents need to continually learn and perform an enormous number of complex tasks. Sometimes very similar contexts require totally different actions. For instance, while soccer and handball both require to put a ball in a goal which is guarded by a keeper and some defenders, soccer requires to manipulate the ball with the feet while handball requires to manipulate the ball with the hands. In such contexts, it is important to separate stimulus-action representations between the two tasks as much as possible in order to avoid interference. However, at other times, two different contexts nevertheless require partially similar actions. Despite the fact that tennis requires to play a ball over a low-hanging net and badminton requires to play a shuttle over a higher placed net, one can partially generalize the action of swinging the racket between the two sports. Thus, in these cases, an agent can significantly benefit from partially sharing knowledge between the two tasks.

48

49

50

51

52

53

54

55

56

57

58

59

60

61

62

Previous research (Baxter, 2019; Franklin & Frank, 2018; Musslick et al., 2017; Vaidya, Jones, Castillo, & Badre, 2021; Zambaldi et al., 2018) indeed illustrated that sharing task representations significantly improves learning and generalization across tasks, two hallmarks of human flexibility. However, sharing task representations in a neural network severely impacts the network's ability to perform more than one task at the same time (i.e., to multi-task; Alon et al., 2017; Musslick et al., 2017; Musslick, Saxe, Novick, Reichman, & Cohen, 2020). Moreover, shared task representations leave a network very vulnerable to overwriting previously learned information. This problem is known as catastrophic interference (French, 1999). In contrast, a network that develops separated task representations experiences less problems in multi-tasking (Musslick et al., 2020; Tsai, Saxe, & Cox, 2016) and can continually learn without forgetting (Kirkpatrick et al., 2017; Masse, Grant, & Freedman, 2018; McClelland, McNaughton, & O'Reilly, 1995; Verbeke & Verguts, 2019). However, such networks are less able to generalize and as a consequence must learn even very similar tasks (like tennis and badminton) from scratch. In sum, there exists a trade-off between sharing and separating task representations in neural networks (Musslick et al., 2017; Musslick & Cohen, 2020; Sagiv, Musslick, Niv, & Cohen, 2020).

63

64

One popular solution to deal with this sharing-separating trade-off are compositional task representations (Fidler, Boben, & Leonardis, 2009; Franklin & Frank, 2018; Lake et al., 2014; Sugita,

65 Tani, & Butz, 2011; Tubiana & Monasson, 2017; Yang, Joglekar, Song, Newsome, & Wang, 2019).
66 For instance, to a first approximation, knowledge of soccer can be decomposed in two basic building
67 blocks: the goal of the task (getting the ball past the goalkeeper) and the actions (kicking the ball). This
68 allows the agent to generalize the goal when learning to play handball but also to avoid interference by
69 separating the actions between both sports. Hence, a novel task can be learned quickly by recombining
70 building blocks from previously learned tasks. Indeed, generalizing information through compositional
71 task representations received considerable attention in several cognitive domains such as language
72 (Irsoy & Cardie, 2014; Irsoy & Cardie, 2015; Lake et al., 2014) and sensorimotor learning (Butz,
73 Achimova, Bilkey, & Knott, 2021; Butz, Bilkey, Humaidan, Knott, & Otte, 2019; Sugita et al., 2011).
74 Nevertheless, it is not clear which neural network configurations could learn such compositional
75 representations (Hupkes, Dankers, Mul, & Bruni, 2020; Lake & Baroni, 2018; Lake, Ullman,
76 Tenenbaum, & Gershman, 2017), and what the resulting compositional representations would look like.
77 The current work aims to build upon previous cognitive and computational work to investigate which
78 cognitive architectures can balance shared and separated task representations in typical cognitive tasks,
79 and what type of representations successful architectures would develop.

80 In cognitive science, the ability to perform one task while eliminating interference from other
81 tasks, is known as cognitive control. Influential theoretical work (Miller & Cohen, 2001), suggests that
82 cognitive control is implemented as a top-down modulatory signal that prioritizes relevant information
83 processing in other processing areas. Specifically, it has been suggested that the human prefrontal cortex
84 sends modulatory signals to more posterior processing areas; such signals excite task-relevant
85 processing pathways and inhibit task-irrelevant processing pathways (Aben, Calderon, Van den
86 Bussche, & Verguts, 2020). Hence, the prefrontal cortex can separate information by inhibiting all
87 processing that might interfere with the current task. This approach has proven fruitful to explain human
88 behavior in cognitively demanding tasks (Abrahamse, Braem, Notebaert, & Verguts, 2016; Botvinick,
89 Braver, Barch, Carter, & Cohen, 2001; Cohen, Dunbar, & McClelland, 1990; Verbeke & Verguts,
90 2019). However, as noted above, a complete separation between task representations would be
91 inefficient. Indeed, in some cases the network might benefit from information transfer between similar
92 tasks.

93 To study the balance between sharing and separation, we consider the nature of top-down
94 signals. Interestingly, there exist some crucial differences in the literature with respect to how top-down
95 modulation is implemented. For instance, while some research treats the top-down signal as any other
96 input signal and add all inputs together (Cohen et al., 1990), other research has treated the top-down
97 signal as multiplicative (Masse et al., 2018; O'Reilly & Frank, 2006), which allows to effectively shut
98 down (multiply by zero) activity for irrelevant neurons. Additionally, while in most research the
99 modulatory signal is adapted to the needs of the current task (Botvinick et al., 2001; Cohen et al., 1990;
100 Verguts & Notebaert, 2008), other work (Bouchacourt & Buschman, 2019; Masse et al., 2018)
101 illustrated that also random, non-adaptive modulatory signals can be sufficient to allow optimal
102 performance on complex tasks. Hence, random signals can often meet performance of learned signals,
103 while requiring far less computational constraints. Moreover, because less parameters need to be
104 learned, these random modulatory signals are often faster in learning to process novel inputs. More
105 generally, random signals have proven to be useful in constructing powerful neural networks (Lillicrap,
106 Cownden, Tweed, & Akerman, 2016; Maass, Natschläger, & Markram, 2002). Thus, top-down
107 modulation signals differ in whether they are additive or multiplicative and whether they are adaptive
108 or non-adaptive.

109 The current work provides a systematic investigation of different types of modulation signals
110 in balancing the trade-off between shared and separated representations. Specifically, we propose four
111 approaches for modulation. In a first approach, non-adaptive additive modulation (N+ network) is
112 applied. Here, for each task, a different random top-down signal contributes to the activity patterns in
113 an additive manner. Second, in adaptive additive modulation (A+ network), top-down input is also
114 added to the network. However, in this approach, the top-down input is treated like any other task-
115 processing input in the sense that top-down weights are susceptible to the same (backpropagation)
116 learning rules as the regular task-processing weights. Third, in non-adaptive multiplicative modulation
117 (Nx network), the network inhibits and/or excites a random proportion of pathways in every task context
118 by multiplying activation with zero (inhibition) or a random positive value (excitation). Fourth, in
119 adaptive multiplicative modulation (Ax network), the network learns which processing pathways to
120 excite or inhibit.

121 Since previous work illustrated that the impact of shared representations depends on the nature
122 of the task environment (Musslick et al., 2017), networks are tested on three different types of input
123 (discrete low-dimensional, continuous low-dimensional, and continuous high-dimensional; see also
124 Figure 1). For each input type, we consider a number of tasks that differ in the amount of overlap of
125 their stimulus-action mappings. Interestingly, for artificial agents, there is more catastrophic
126 interference when trained in a blocked fashion. In contrast, blockwise training appears beneficial for
127 human agents (Flesch, Balaguer, Dekker, Nili, & Summerfield, 2018). To evaluate each network's
128 ability to overcome interference, we thus trained our artificial networks in a blocked fashion. In sum,
129 we test the four modulation signals on a task that requires them to optimally balance the transfer
130 (sharing) and avoidance of interference (separating) between tasks. Network performance is evaluated
131 in terms of accuracy and the ability to find the optimal amount of sharing between task representations.

132

133 2. Methods

134 2.1 The network

135 Our network (Figure 1a) consists of an Input, Hidden, and Output layer. Information flows in
136 a feedforward manner from Input to Hidden to Output layer. All neurons in each layer are fully
137 connected to all neurons in the next layer. Neurons in the Input layer are divided in a Stimulus group
138 and a Task group. Activation at the Hidden layer is a combination of input from the Stimulus group and
139 a modulatory signal from the Task group. In analogy to previous work, we use

$$140 \quad \mathbf{H} = f(\mathbf{S}\mathbf{W}_{s,h} + \mathbf{T}\mathbf{W}_{t,h}) \quad (1)$$

140

141 for additive modulation (e.g., Cohen et al., 1990) and

$$142 \quad \mathbf{H} = f(\mathbf{S}\mathbf{W}_{s,h}) \otimes g(\mathbf{T}\mathbf{W}_{t,h}) \quad (2)$$

142

143 for multiplicative modulation (e.g., Masse et al., 2018). However, see the Supplementary materials for
144 additional simulations with other implementations of modulation. In these equations, \mathbf{H} , \mathbf{S} and \mathbf{T} are
145 vectors representing activation in the Hidden, Stimulus and Task group respectively. A weight matrix

146 between layers is represented by W . The symbol \otimes represents elementwise multiplication. The
147 functions $f()$ and $g()$ represent (elementwise) nonlinear activation functions. In the main text we
148 consider simulations in which $f()$ represents a sigmoid activation function:

149

$$\text{sig}(\mathbf{XW}_{x,j}) = \frac{1}{1 + e^{-(\mathbf{XW}_{x,j})}} \quad (3)$$

150

151 and $g()$ represents a RELU activation function:

152

$$\text{RELU}(\mathbf{XW}_{x,j}) = \max(0, (\mathbf{XW}_{x,j})) \quad (4)$$

153

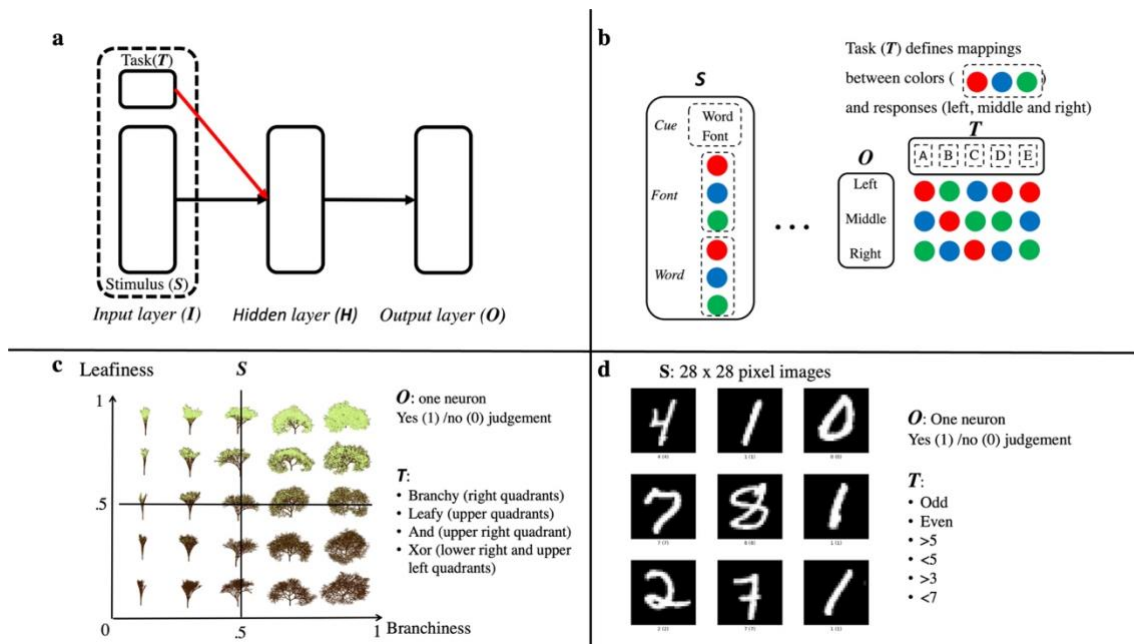
154 In these equations, \mathbf{X} is a (row) vector representing activity in the sending layer and $\mathbf{W}_{x,j}$ represents a
155 weight matrix between the sending (x) and receiving (j) layer. Thus, Hidden neurons with a negative
156 weight from the active Task neuron are gated out (activation multiplied by 0), while activation of
157 Hidden neurons with a positive weight, are multiplied by a positive value. The Supplementary materials
158 present additional simulations in which different combinations of sigmoid and RELU functions are
159 explored. Activation at the Output layer (\mathbf{O}) simply follows $\mathbf{O} = \text{sig}(\mathbf{HW}_{h,o})$. After each trial, weights
160 are adapted by the backpropagation learning rule (Rumelhart, Hinton, & Williams, 1986):

161

$$\Delta \mathbf{W}_{x,j} = -\alpha \times \frac{\partial E}{\partial \mathbf{W}_{x,j}} \quad (5)$$

162

163 in which again x represents the sending layer and j represents the receiving layer. The parameter $\alpha > 0$
164 represents a learning rate, and $\frac{\partial E}{\partial \mathbf{W}_{x,j}}$ is the (partial) derivative of the error (E) with respect to the weights
165 (W).



166

167 **Figure 1. Network architecture and simulations.** *a*: General network architecture. The network consists
 168 of three layers. Information flows in a feedforward manner from Input to Hidden to Output layer. The Input
 169 layer is divided in a Stimulus and Task group. The Task group sends a modulation signal (red arrow). We
 170 evaluate four different types of modulation and test the network on three types of stimulus datasets (b-d). *b*:
 171 Stroop (discrete) dataset. Stimuli are a combination of a cue, a font (color) and a (color) word. The cue
 172 indicates which other dimension (word or font) is relevant for responding. Five tasks are defined in which
 173 the mapping between three response options and three values for color (in font and word) are changed.
 174 Mappings are represented in the panel. *c*: Trees (continuous low-dimensional) dataset. The stimulus figure
 175 is adopted from Flesch et al. (2018). Current work has coded this dataset with two neurons that can take on
 176 any value between 0 and 1. Four tasks are defined in which the network needs to give a yes or no judgement
 177 (one response neuron). *d*: MNIST (continuous high-dimensional) dataset. Here, stimuli are 28 x 28 pixel
 178 images of handwritten digits from 0 to 9. Examples are taken from
 179 <https://www.tensorflow.org/datasets/catalog/mnist>. We defined six possible tasks in which again the
 180 network needs to give a yes/no judgement.

181 2.2 Datasets

182 The network was tested on three datasets (Figure 1b-d), allowing us to evaluate several
 183 combinations of input and task type. Note that the size of the Input, Output and Task layers were adapted
 184 depending on the input dataset. The first dataset had discrete (binary) low-dimensional input patterns.
 185 Specifically, we consider the classic cognitive control Stroop task (Stroop, 1935). See Figure 1b for an
 186 illustration of the network specifics for this dataset. Here, on each trial a (color) word is presented
 187 (“red”, “green” or “blue”) in a particular font (color) (red, green or blue). Additionally, a cue is provided

188 telling the agent to respond either to the word or to the font dimension. The task consists in learning
189 mappings between colors (red, green and blue) and response buttons (left, middle, right). Crucially,
190 both stimulus dimensions can provide congruent evidence (e.g. “red” presented in red) or incongruent
191 evidence (“red” presented in blue). In the latter case, the correct response depends on the cue dimension
192 (respond to red when cue is word and to blue when cue is font). In terms of the network, we consider 8
193 input neurons (2 cues, 3 words and 3 colors; see also Figure 1b). Here, each stimulus consists of the
194 activation (input value = 1) of 3 (a cue, a word and a font) out of 8 Stimulus neurons, resulting in 18 (2
195 instructions \times 3 fonts \times 3 words) possible stimuli. Additionally, we activate one Task neuron on every
196 trial, which determines the appropriate mappings between stimuli and responses. In this task, the Output
197 layer consists of 3 neurons. On each trial, the Output neuron with the highest activation ($\text{argmax}(\mathbf{O})$) is
198 considered to be the network response. Depending on the task, each color value (red, green or blue) was
199 mapped to one of the neurons in the Output layer. Specifically, we define five tasks (see also Figure
200 1b). Here, tasks A, B and C share no stimulus-action mappings. Task D represents a mix of tasks A, B
201 and C. Specifically, D shares exactly 1/3 of stimulus-action mappings with all three other tasks. The
202 last task E shared all stimulus-action mappings with A but activated a different neuron in the Task group
203 (in a sense, A and E are synonyms). Note that we call this a Stroop task because the input consists of
204 font and word input where one dimension was relevant; we did not mimic the imbalance between color
205 naming and word reading that appears in typical Stroop tasks.

206 The second dataset is the Trees dataset (see also Flesch et al., 2018). Specifics for this dataset
207 are presented in Figure 1c. In the Trees dataset, there are two Stimulus neurons which can take on any
208 value in a range of 0 to 1 (continuous low-dimensional input). One Stimulus neuron represents the
209 ‘leafiness’ of a tree and the other Stimulus neuron represents the ‘branchiness’ of the tree. The Output
210 layer contained only one neuron. For this dataset, the network has to make a yes (output = 1) or no
211 (output = 0) judgement. We defined four different tasks for this input type. One task was to respond yes
212 to leafy trees (leafiness $>.5$), a second task was to respond to branchy trees (branchiness $>.5$), a third
213 task required the network to respond to trees that were both leafy and branchy (AND task), and the
214 fourth task consisted of responding to trees that were either leafy or branchy (but not both; XOR task).
215 Note that for this dataset there were no completely (100%) dissimilar tasks. The Leafy and Branchy

216 task share 50% of stimulus-action mappings with each other but also with the AND and XOR tasks. The
217 AND and XOR task share 25% of mappings with each other.

218 The third dataset consisted of images (continuous, high-dimensional input). More specifically,
219 we used the MNIST data set (LeCun, Cortes, & Burges, 2010) which contains grey-scaled images (28
220 x 28 pixels) of handwritten digits from 0 to 9. Again, the Output layer consisted of one neuron. For this
221 input type, 6 different tasks were provided. One task was to respond to odd digits (i.e., output = 1 for
222 odd digits; output = 0 for even digits); another task required a response to even digits. A third and fourth
223 task required the network to respond to digits that were respectively larger or smaller than 5. The fifth
224 task consisted of responding to digits larger than 3 and the sixth task was to respond to digits smaller
225 than 7. This resulted in a complex pattern of overlap between the different tasks. Tasks vary from 100%
226 dissimilar (odd and even), to only 20% dissimilar (>3 and >5; <5 and <7).

227 **2.3 Simulations**

228 As described before, four versions of the network were simulated. Activation at the Hidden
229 layer follows Equation (1) for additive modulation networks (N+ and A+), and Equation (2) for
230 multiplicative modulation networks (Nx and Ax). In adaptive modulation networks (A+ and Ax), the
231 weights between the Task group and Hidden layer are learned by the backpropagation rule (Equation
232 (5)), just like the other weights. In non-adaptive modulation networks (N+ and Nx), the weights between
233 the Task group and Hidden layer are fixed at their initial (random) values. All weights are initialized
234 with a random value drawn from the normal distribution $N(0, 1)$. Only for the Ax network, modulating
235 weights (between Task and Hidden layer) had an initial random value drawn from the uniform
236 distribution $U(0, 1)$, such that $\text{RELU}(\mathbf{T}) > 0$ (all gates open) at the first trial. This set up provides the
237 most optimal initialization for each network. We illustrate network performance with other weight
238 initialization distributions in the Supplementary materials.

239 All four versions of the network were tested on all three data sets. Additionally, we explored
240 different learning rates (α) and shapes of Hidden layer. Also the shapes of the Input, Output and Task
241 layers were adapted depending on the input dataset. For the Stroop and Trees input datasets, α took on
242 6 values ranging from 0 to 1 in steps of .2. We explored the network with one Hidden layer of either 12

243 or 24 neurons. For the MNIST dataset we used lower learning rates. Here, α took on 6 values ranging
244 from 0 to .1 in steps of .02. For this data set, we explored performance with one Hidden layer of 400
245 neurons; and also with two Hidden layers (300 and 100 neurons respectively) and three Hidden layers
246 (200, 100 and 100 neurons respectively). Note that for this dataset, the total number of Hidden neurons
247 did not differ between architectures. Activation at the first Hidden layer (H_1) followed Equation (1) or
248 (2) for additive or multiplicative networks respectively. In standard simulations, activation at the second
249 and third Hidden layer followed: $H_i = sig(H_{i-1}WH_{i-1}, H_i)$, in which i is the index of the Hidden layer.
250 Hence, the Task modulation signal was not sent directly to the deeper Hidden layer(s). However, for
251 completeness we also explored network performance (with two hidden layers) when the Task signal
252 was sent to only the second hidden layer, to both hidden layers or to none of the hidden layers. Results
253 of these simulations are presented in section 3.5.

254 For every combination of α and shape of the Hidden layer, 25 simulations ($N = 25$) were
255 performed for each dataset. For each simulation, 1200 or 12000 inputs were randomly sampled for the
256 Trees and MNIST datasets respectively. Since there were only 18 stimuli (input patterns) for the Stroop
257 dataset, we chose to repeat these 18 stimuli 75 times in each simulation, resulting in 1350 trials.
258 Additionally, we randomly shuffled the order of tasks before a simulation. In a next step, we divided
259 the sampled input patterns over 3 repetitions (450, 400 or 4000 trials per block for the Stroop, Trees
260 and MNIST dataset respectively). In every repetition, the network was trained (training phase)
261 blockwise on each task, using the predetermined input sample and order of tasks. Thus, each task was
262 repeated 3 times in a blocked fashion. At the end of the third block, weights were frozen, and the
263 network was tested (test phase). For this test phase a new order of tasks was generated. Each task was
264 tested for one block of trials. For this purpose, 100 or 500 new inputs were randomly sampled from the
265 Trees and MNIST datasets respectively. For the Stroop dataset, no new inputs could be generated so
266 we repeated the 18 possible inputs 5 times, resulting in 90 trials.

267 **2.4 Analyses**

268 *2.4.1 Accuracy*

269 To investigate whether networks suffered from catastrophic interference during learning, we
270 computed accuracy for each task repetition (averaged over all tasks). Networks that suffer from
271 catastrophic interference would need to relearn a task on every repetition because they would learn
272 other tasks in between. Hence, such a network would not improve over task repetitions.

273 Next, we investigated the network's ability to balance separating representations with sharing
274 representations. More specifically, we computed accuracy for each task during the test phase. For this
275 analysis we mainly focus on the Stroop dataset but we present results for the other datasets as well. The
276 Stroop dataset is optimally suited for this analysis since there is a larger variation in (dis)similarities
277 between tasks (see also the objective dissimilarity table in Figure 2) than is the case for the other
278 datasets. More specifically, five tasks were proposed for the Stroop dataset. As described in section 2.2,
279 three of them (A, B and C) did not share any stimulus-action mappings and thus can be totally separated.
280 Tasks A and E however, share all stimulus-action mappings and can be fully shared. Additionally, task
281 D shares 1/3 of its stimulus-action mappings with all other tasks. On the one hand, a full sharing of task
282 representations would allow the network to exploit the shared mappings between A, D and E but lead
283 to catastrophic interference in tasks B and C, illustrated by a strong decrease of accuracy in tasks B and
284 C compared to A, D and E. On the other hand, a full separation of tasks would improve accuracy of
285 tasks B and C (by less interference), but would also eliminate the advantage of the full overlap between
286 A and E and the partial overlap between D and the other tasks. Hence, accuracy would be the same for
287 all tasks. Importantly, when the network is only able to fully share or separate information it would
288 benefit from the full overlap between A and E but would not benefit from the partial overlap between
289 task D and the other tasks. In sum, an optimal network would find a balance between sharing and
290 separating, resulting in an improved accuracy for tasks A, D and E while minimizing the dip in accuracy
291 for tasks B and C.

292 To evaluate overall performance of the networks we also computed accuracy during the test
293 phase for all learning rates and all tasks.

294 *2.4.2 Representational dissimilarity*

295 In order to analyze to what extent the networks shared or separated stimulus-action mappings
296 across tasks, we computed how dissimilarity between tasks in terms of stimulus-action mappings was

297 represented in the network. This analysis considers several steps. An overview of these steps in the
298 context of the Stroop dataset is provided in Figure 2.

299 In a first step, we computed for each simulation the objective dissimilarity between stimulus-
300 action mappings across tasks. Specifically, we computed a matrix where rows and columns represent
301 the tasks, and each cell contains the proportion of stimuli that were matched with a different action
302 across the two respective tasks (row and column).

303 A second step was to compute the representational dissimilarity within the network. For this
304 purpose, we first computed the mean activation at Hidden layer for each stimulus (18 Stroop stimuli, 4
305 quadrants of branchy-leafy space and 10 digits in MNIST dataset) in each task across trials. Then the
306 difference between task representations was extracted by computing the mean Euclidean distance for
307 two tasks $T1$ and $T2$. Here,

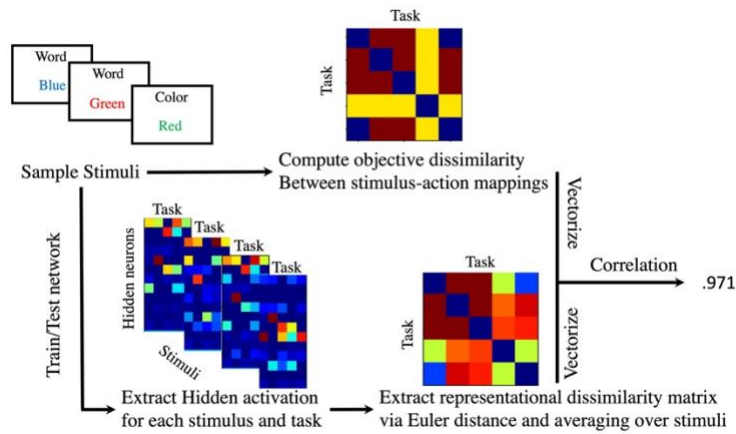
308

$$Dissimilarity_{T1,T2} = \sum_S^{nStim} \|\mathbf{H}_{T1}^S - \mathbf{H}_{T2}^S\| / nStim \quad (6)$$

309

310 in which \mathbf{H}_{T1}^S and \mathbf{H}_{T2}^S are vectors of length $nHidden$, representing the average activity for all Hidden
311 neurons when stimulus S was presented to the network. Hence, we compute the Euclidean distance
312 (indicated by $\|\cdot\|$) for each stimulus (S) and each task pair ($T1, T2$). This distance is then averaged
313 over all possible stimuli ($nStim$) to obtain one dissimilarity matrix of Hidden representations between
314 tasks.

315 In a third and last step we compared the objective dissimilarity to the representational
316 dissimilarity. Specifically, we reshaped both matrices to vectors and computed the Spearman rank
317 correlation coefficient between these vectors. This resulted in one value of the dissimilarity correlation
318 between objective task dissimilarity and a network's representational task dissimilarity.



319

320 **Figure 2. Methods.** Illustration of the different steps in the representational dissimilarity analyses. Examples
321 are shown for one simulation of the Stroop dataset with a learning rate of .6 and 12 Hidden neurons.

322 2.4.3 Neural activation analyses

323 We performed two additional analyses to gain more insight into how the different modulatory
324 signals organize Hidden layer activity. For this purpose, we again computed for each task the mean
325 activation at Hidden layer for each stimulus, resulting in a matrix with size $(nStim, nTask, nHidden)$.
326 First, we investigated the distribution of activation for all stimuli and tasks across the Hidden neurons.
327 Second, in order to visualize the network representations for each task, we reduced Hidden layer
328 dimensionality via principal component analysis. For this purpose, we entered the activation matrix
329 with size $(nStim, nTask, nHidden)$ into the principal component analysis and approximated it by a matrix
330 of size $(nStim, nTask, 2)$. As a result, we could plot the representation of each stimulus in each task in
331 a two-dimensional space.

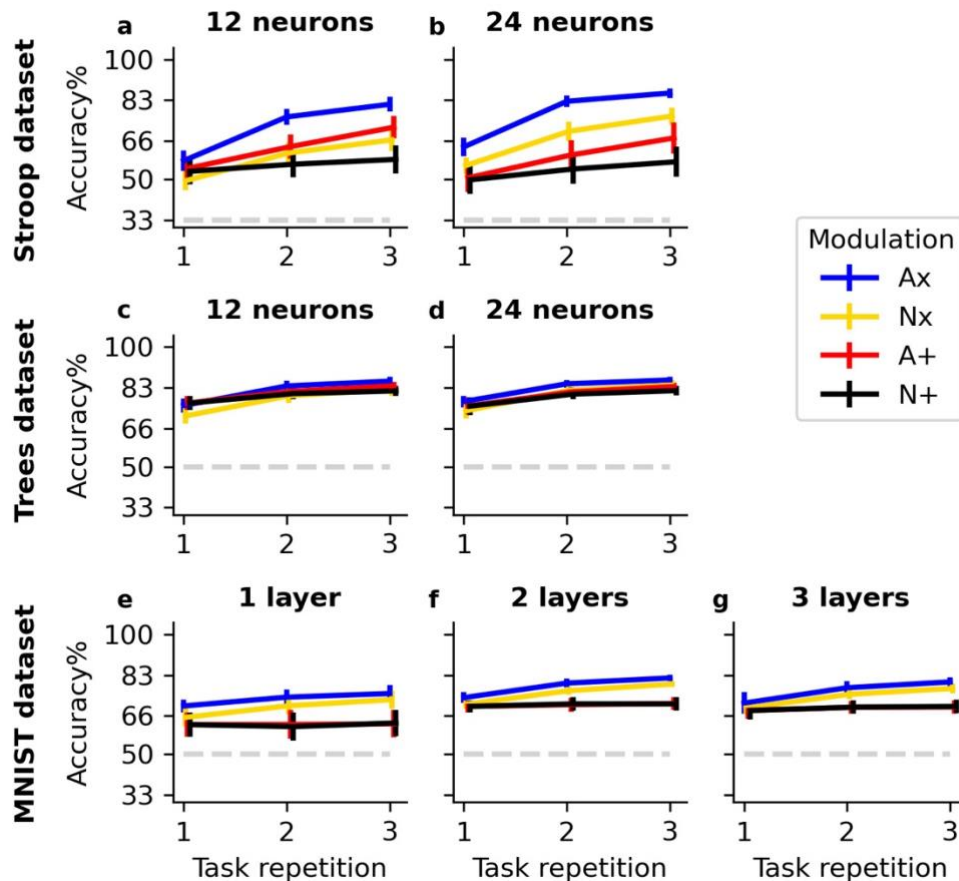
332

3. Results

333 3.1 Accuracy

334 First, we evaluated the networks' ability to separate task representations. For this purpose, we
335 investigated whether average accuracy (during the training phase) increased over task repetitions.
336 Networks that do not separate task sets suffer from catastrophic interference because they overwrite
337 mappings of one task by the mappings of another task. As a result, such networks need to relearn the
338 original task when it is presented again, and do not show any improvement over task repetitions. In
339 Figure 3, it is observed that accuracy hardly improves for the additive networks (A+ and N+). Thus,
340 these networks severely suffered from catastrophic interference. In contrast, for multiplicative

341 modulation networks, in particular for the Ax network, there was a significant improvement over task
 342 repetitions. Thus, multiplicative modulation seems more efficient in separating task representations,
 343 rendering them less vulnerable to catastrophic interference during learning.

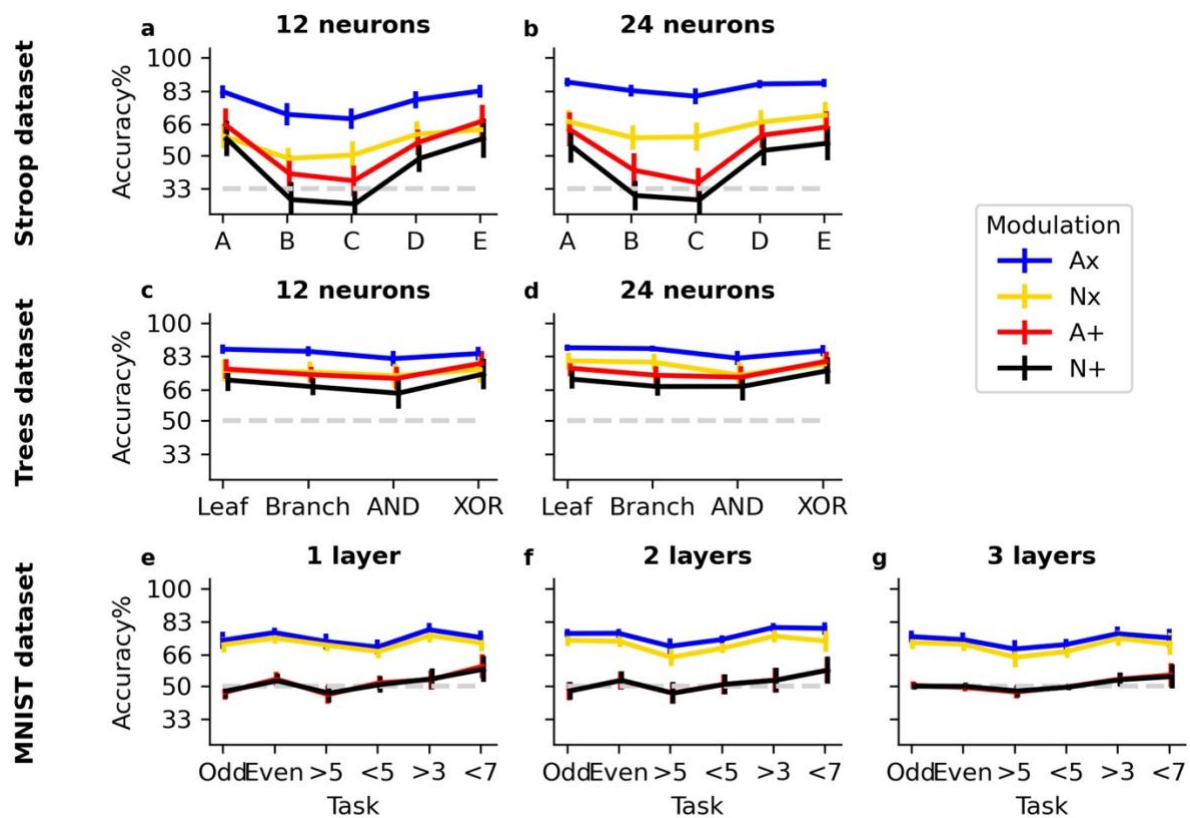


344

345 **Figure 3. Accuracy in training phase per task repetition.** Lines illustrate mean accuracy for each task
 346 repetition during the training phase averaged across all learning rates (α), all tasks and all simulations. Bars
 347 indicate 95% confidence intervals over 25 simulations. The dashed lightgrey line indicates chance level
 348 accuracy. Results are shown for different datasets (rows) and different shapes of Hidden layer (columns).

349 Second, we zoomed in on accuracy for each task during the test phase. Here, we focus mainly
 350 on the Stroop dataset (see section 2.2) because the Stroop dataset has a broader range of dissimilarities
 351 between tasks. Specifically, tasks A, B and C have completely dissimilar mappings, task D has a partial
 352 overlap of 1/3 with all other tasks and task E shares all mappings with task A. An optimal network
 353 would find a balance between sharing and separating, resulting in an improved accuracy for tasks A, D
 354 and E while minimizing the dip in accuracy for tasks B and C (see also section 2.4.1). In Figure 4a,b
 355 we observe a strong dip in accuracy for tasks B and C when the modulation signal was additive. This

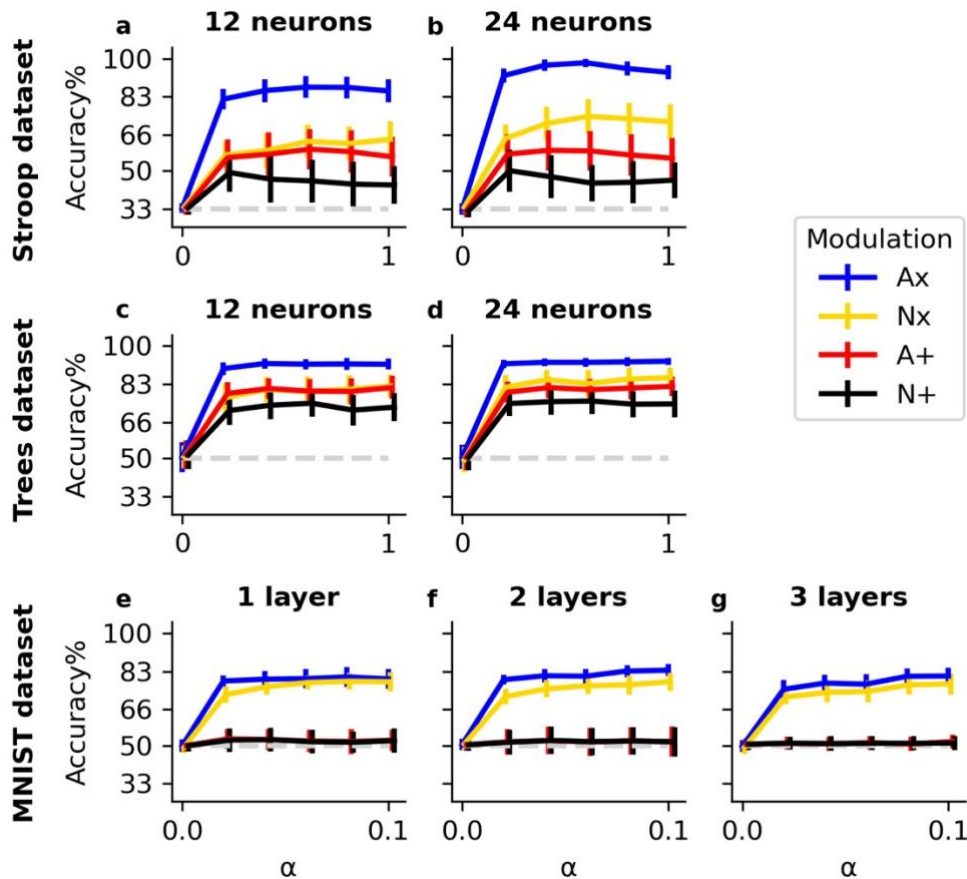
356 suggests that additive modulating signals are well suited for sharing task representations, but less so for
 357 separating task representations. This dip in accuracy for tasks B and C is less strong for the
 358 multiplicative modulation networks. Importantly, the Nx network has an approximately equal accuracy
 359 for all tasks (Figure 4a,b). This suggests that the Nx network has strongly separated task representations,
 360 which did not allow that network to benefit from overlap between task mappings across the different
 361 tasks. The Ax network is clearly the network that was able to optimally balance the separation and
 362 sharing of task representations, showing an advantage in accuracy for all tasks compared to the other
 363 networks, and only a small dip for tasks A and B. Note that although task D only had a partial overlap
 364 with other tasks, accuracy is equally high as for tasks A and E which fully overlapped. Hence, the Ax
 365 network does not treat sharing or separation as an all-or-none process, but also captures partial overlap.



366
 367 **Figure 4. Accuracy in test phase per task.** Lines illustrate mean accuracy during the test phase for each
 368 task, averaged across all learning rates (α) and all simulations. Bars indicate 95% confidence intervals over
 369 25 simulations. The dashed lightgrey line indicates chance level accuracy. Results are shown for different
 370 datasets (rows) and different shapes of Hidden layer (columns).

371 We also show results for the other datasets but these are less informative in this respect,
372 because there is no strong variability in objective task dissimilarity (see section 2.2). For the Trees
373 dataset (Figure 4 c,d) there was an average objective dissimilarity of 50% for the leafy and branchy
374 task, and an average dissimilarity of 41.5% for the AND and XOR tasks. For the MNIST dataset (Figure
375 4e-g) there was a strong variability of dissimilarity between tasks themselves (20-100%), but when
376 averaged over all tasks, the range of dissimilarity between one task and all other tasks was rather small
377 (between 56 and 64%). Despite the absence of variability in overall dissimilarity between tasks, it is
378 also clear for the Trees (Figure 4c, d) and MNIST (Figure 4e, f) dataset that the Ax network performs
379 best.

380 This suggestion that the Ax network is best able to find a balance between sharing and
381 separating task representations, is supported by the fact that this network reaches a higher accuracy
382 overall when we analyze accuracy over all tasks during the test phase. In Figure 5, it is observed that
383 the Ax network outperforms all other networks for all learning rates, all shapes of Hidden layer and all
384 datasets. The non-adaptive additive (N+) network performs worst. The non-adaptive multiplicative
385 modulation (Nx) network and the adaptive additive (A+) network perform in between these other
386 networks. Here, the Nx modulation network seems to obtain an advantage over the A+ network when
387 there are more Hidden neurons (Figure 5b,d) and for high-dimensional (MNIST; Figure 5e,f) input
388 datasets. In sum, multiplicative modulation outperforms additive modulation, and adaptive modulation
389 outperforms non-adaptive modulation.



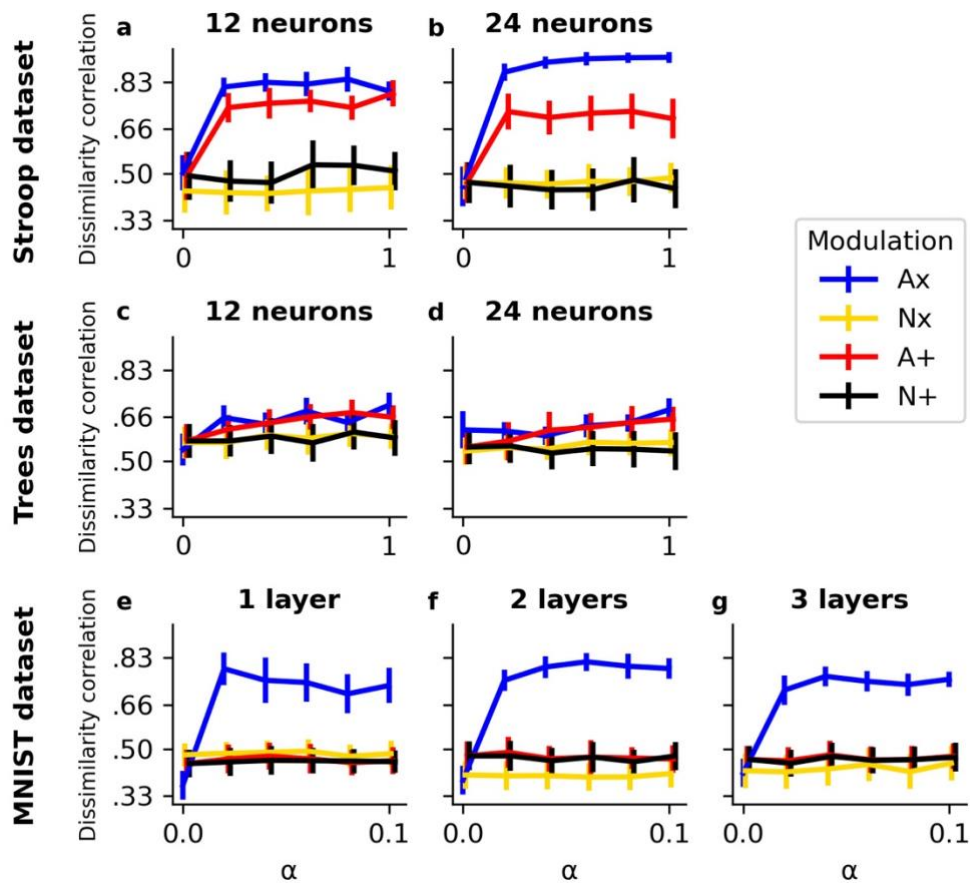
390

391 **Figure 5. Accuracy in test phase per learning rate (α).** Lines illustrate mean accuracy during the test
 392 phase for each value of α , averaged across all tasks and all simulations. Bars indicate 95% confidence
 393 intervals over 25 simulations. The dashed lightgrey line indicates chance level accuracy. Results are shown
 394 for different datasets (rows) and different shapes of Hidden layer (columns).

395 3.2 Representational dissimilarity

396 We next investigate whether objective dissimilarity of stimulus-action mappings between
 397 tasks was represented in the network. For this purpose, we computed for each network simulation a
 398 representational dissimilarity matrix and correlated this matrix elementwise with an objective
 399 dissimilarity matrix of stimulus-action mappings between tasks (see section 2.4.2 and Figure 2 for
 400 details). Results of this analysis are shown in Figure 6. As was already suggested by the accuracy results
 401 (section 3.1), the Ax network was clearly better at extracting the objective dissimilarity between tasks.
 402 Interestingly, the A+ network was also (although less strongly) able to capture the objective overlap
 403 between tasks for the Stroop and Trees input datasets (Figure 6a-d), but not for the MNIST dataset
 404 (Figure 6e-g).

405 For the MNIST dataset, we simulated a network with one Hidden layer (Figure 6e), one with
 406 2 Hidden layers (Figure 6f) and one with three Hidden layers (Figure 6g). Overall, there does not seem
 407 to be a strong benefit for dividing the (same number of) Hidden neurons over multiple layers in the
 408 current setup. However, only the first Hidden layer received a modulation signal. In section 3.5 we
 409 present results for simulations that modulated deeper and/or more hidden layers.

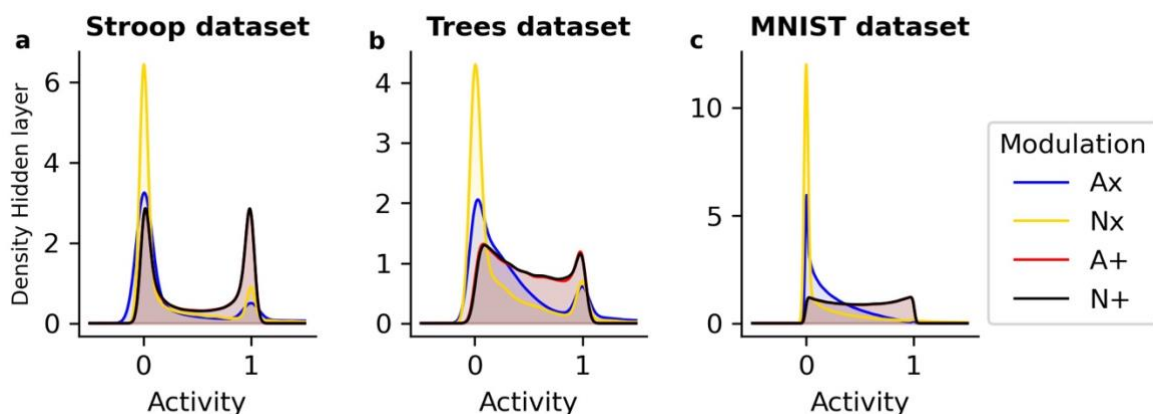


410
 411 **Figure 6. Correlation of objective and representational dissimilarity between tasks.** Lines illustrate the
 412 mean task dissimilarity correlation for each value of α across all simulations. Bars indicate 95% confidence
 413 intervals over 25 simulations. Results are shown for different datasets (rows) and different shapes of Hidden
 414 layer (columns).

415 3.3 Neural activation analysis

416 To provide additional insight into how the different modulation signals organize Hidden layer
 417 activity, Figure 7 shows the distribution of activation at the Hidden layer for all networks and datasets.
 418 This is shown for the networks with 12 Hidden neurons (Stroop and Trees dataset) or 1 Hidden layer
 419 (MNIST dataset). Here, it is observed that activation distributions are strongly bimodal with peaks

420 around 0 and 1. Note that, because of the RELU modulatory signal (see Equations (2) and (4)),
421 activation in the multiplicative modulation networks were theoretically not bound to 1. Nevertheless,
422 also these multiplicative modulation networks show a clear activation bound of 1 after learning.
423 Interestingly, the multiplicative modulation networks illustrate a strong asymmetrical distribution with
424 a higher peak of activity around zero. Especially the Nx network has a high zero-centered peak. This
425 suggests that the Nx network is learning more sparse representations and potentially creates different
426 groups or modules of neurons where each module learns (part of) one task. Hence, in line with what
427 was described before, the Nx network is well suited for separating task representations. The activity
428 distribution of the additive networks is clearly more symmetrical with a higher number of neurons that
429 exhibit strong activity for each stimulus and task. As a result, the additive networks will probably share
430 more neurons for representing stimuli and/or tasks. In line with what we described before, the Ax
431 network illustrates a mixture between the properties of the Nx and additive networks and is therefore
432 optimally suited to balance shared and separated representations.



433
434 **Figure 7. Distribution of activity at Hidden layer.** The distribution of activation at the Hidden layer of the
435 different modulation networks is shown for each dataset.

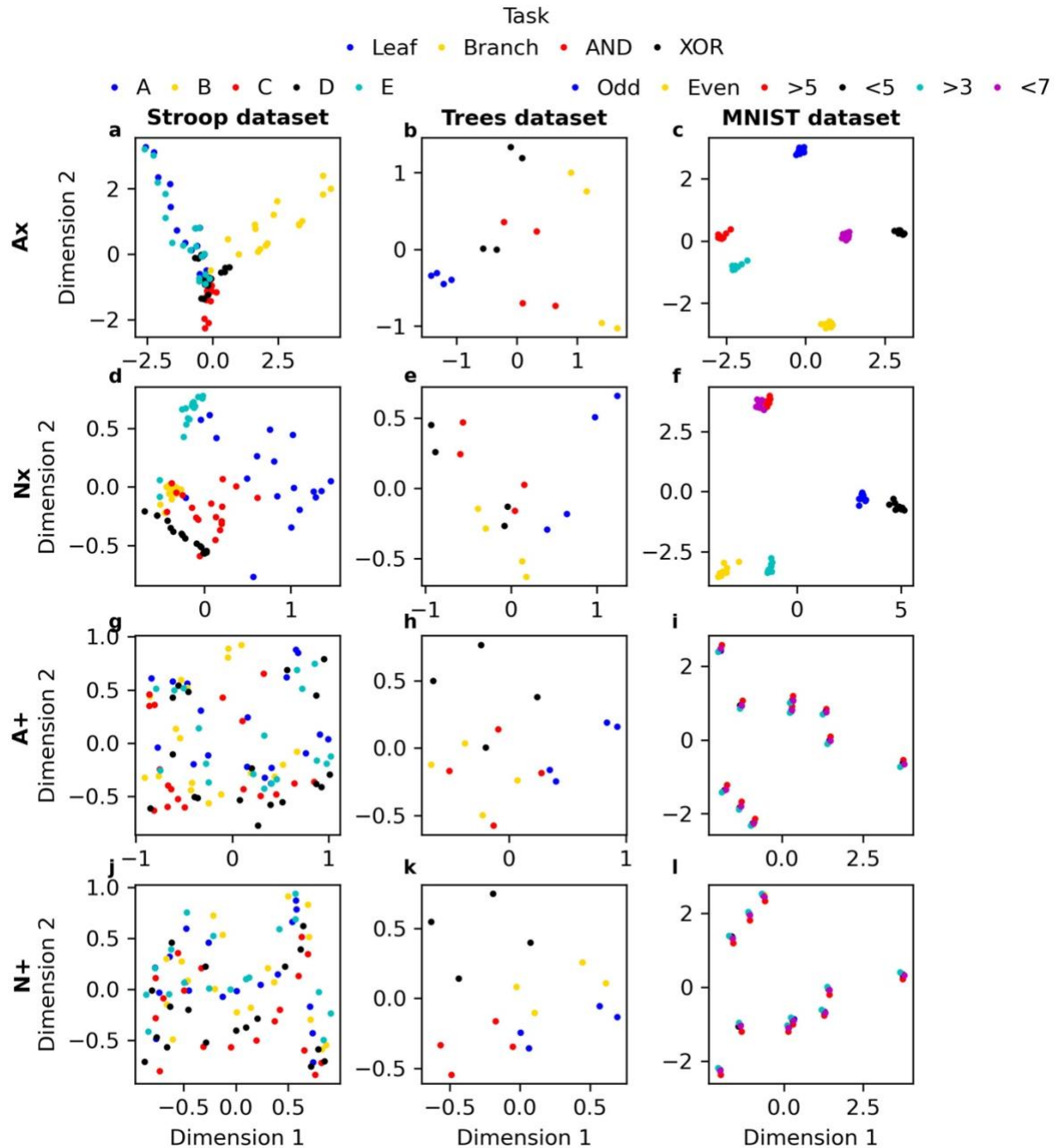
436 For the next analyses, we reduced Hidden layer dimensionality into two principal components
437 with the highest eigenvalues. For the Stroop dataset these components explained on average over all
438 simulations, networks, learning rates and shapes of Hidden layer, 54.34% of the variance (SD = 6.41%).
439 For the Trees dataset, two components explained 71.29% of the variance (SD = 8.16%) and for the
440 MNIST dataset, two components explained 44.95% of the variance (SD = 4.68%). In Figure 8, we show
441 neural representations in the Hidden layer for each stimulus (dots) and each task (colors) on 2

442 dimensions. Notice that this analysis does not allow us to average over simulations. Hence, results are
443 shown for one representative simulation of the network with an intermediate learning rate of $\alpha = .6$ for
444 the Stroop and Trees dataset and $\alpha = .06$ for the MNIST dataset.

445 Generally, results are in line with our previous findings in accuracy and representational
446 dissimilarity analyses. For the Stroop dataset, we observe that the additive modulation networks show
447 a tendency to share neural representations across tasks (Figure 8g,j). In contrast, the Nx network (Figure
448 8d) effectively separates the different tasks but fails to share tasks A and E (blue and green dots) which
449 have no dissimilarities in their stimulus-action mappings. The Ax network however (Figure 8a), shows
450 a remarkable ability in discovering the overall relational structure between tasks. The network finds
451 three orthogonal axes for the three orthogonal tasks A, B and C. Task D which shares stimulus-action
452 mappings with all previous tasks, is placed in between (at the origin of the three axes) the
453 representations of A, B and C. Additionally, the network discovered that task E fully overlaps with task
454 A.

455 For the Trees dataset (Figure 8b,e,h,k), all networks were able to separate task representations.
456 Thus, in contrast to the Stroop input datasets, the additive networks were able to separate task
457 representations for the Trees dataset. This explains why the difference in accuracy between networks
458 was much smaller for the Trees dataset in comparison to other datasets (Figure 5). Note that in this
459 dataset the inputs were significantly less complex (only 2 dimensions) than for the other datasets (18 or
460 $784 (28^2)$ dimensions for the Stroop and MNIST dataset respectively).

461 For the MNIST dataset, the additive networks again fail to separate task representations
462 (Figure 8i,l). Notice that the networks extracted separate representations for the 10 digits (0-9) but
463 shared the digit representations across all tasks. The Nx network (Figure 8f) was able to separate task
464 representations but did not extract a clear relational structure. Again, only the Ax network (Figure 8c)
465 was able to extract the full relational structure of the tasks. Here, two dimensions were extracted by the
466 network. One dimension (Dimension 2) was used to separate the odd from the even tasks, the other
467 dimension (Dimension 1) was used to separate the larger than (>5 and >3) tasks from the smaller than
468 (<5 and <7) tasks.



469

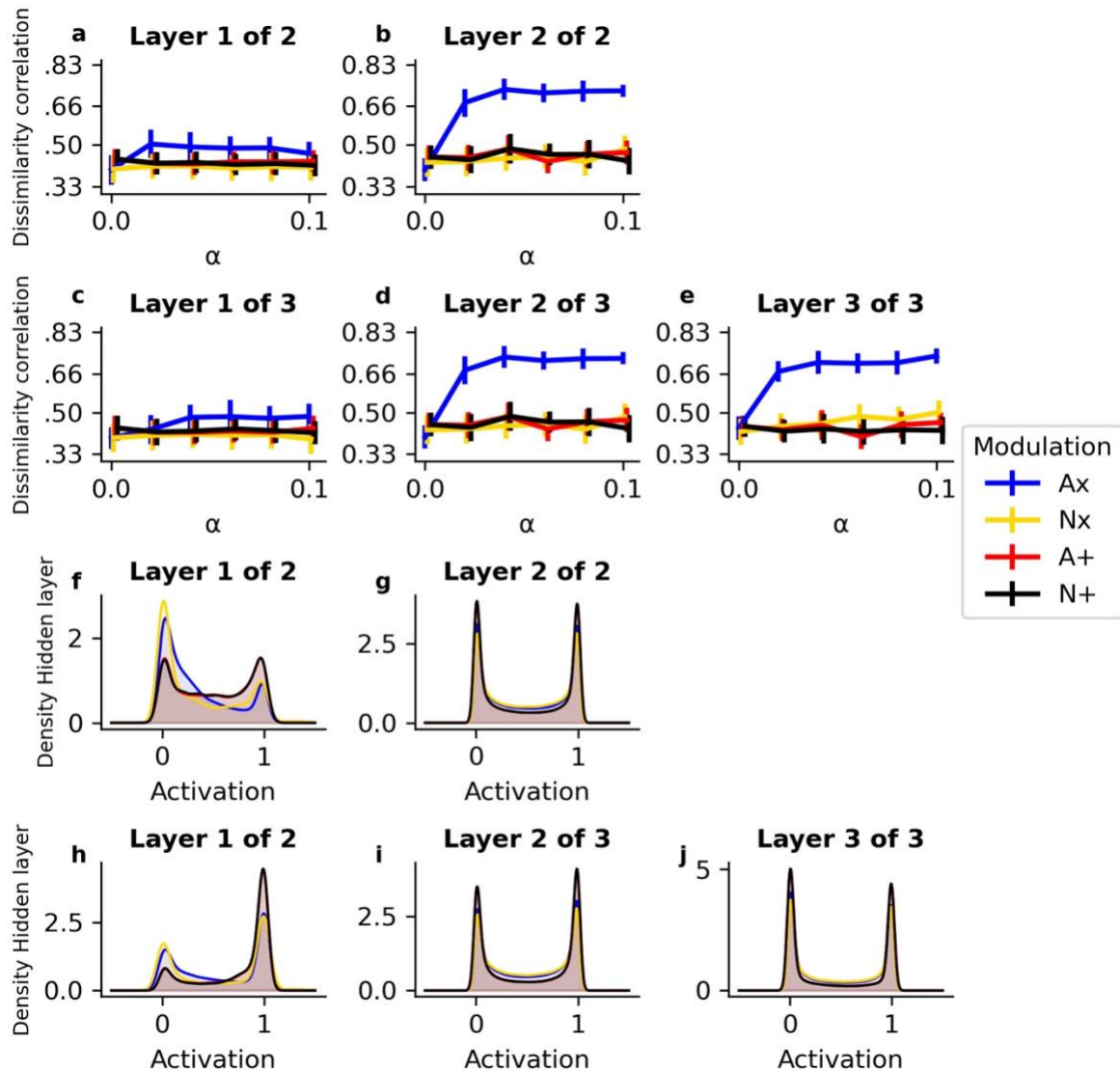
470 **Figure 8. Task representations after principal component analysis.** The neural representation for each
 471 stimulus (dots) and each task (colors) are shown along the first two principal components. This is shown for
 472 a representative simulation and an intermediate learning rate, for all modulation networks (columns).

473 3.4. Multilayer networks

474 To provide more insight into the deeper (more than one Hidden layer) networks, we provide
 475 results of the representational dissimilarity analyses in each layer separately (Figure 9a-e). This is
 476 shown for the two and three Hidden layer networks that were tested on the MNIST dataset. Remarkably,
 477 while the modulation signal is only delivered to the first Hidden layer (Figure 9a,c), the other (second

478 and third but not the first) Hidden layer(s) represent the dissimilarity between tasks better (Figure
479 9b,d,e).

480 Intriguingly, we observe in Figure 9f-j that, in terms of activation, the differences between the
481 modulation networks are more pronounced at the first layer than at the second or third layer. This
482 contrasts with the previous result (Figure 9a-e) that task dissimilarity correlations are more pronounced
483 in the second and/or third Hidden layer(s). However, it is important to keep in mind that separating task
484 representations does not necessarily lead to higher dissimilarity correlations as the different tasks also
485 illustrate significant similarities. This is also emphasized by the fact that the Nx network clearly
486 separates all tasks but does not show a strong dissimilarity correlation. Although it deserves further
487 investigation, it might well be that task mappings are maximally separated in the first Hidden layer and
488 then (compositionally) recombined in the deeper layers.



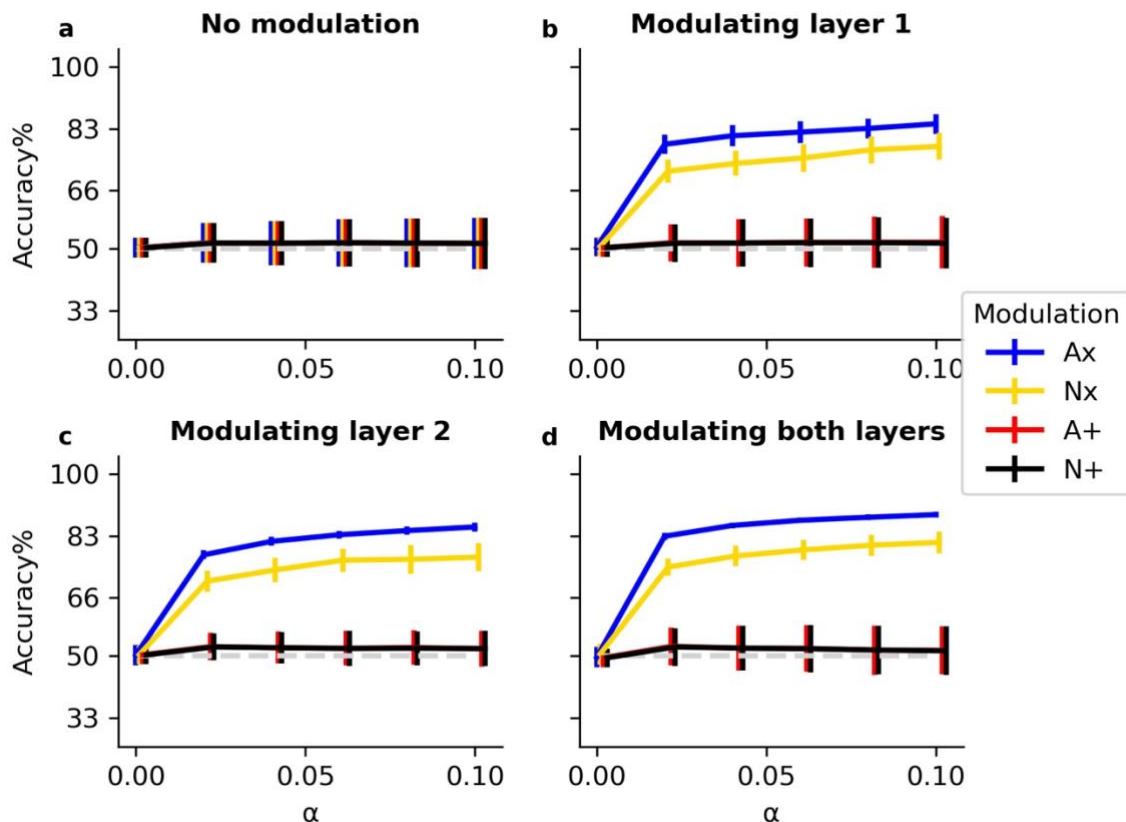
489

490 **Figure 9. Hidden layer activity for multilayer networks.** The upper two rows (panels a-e) illustrate the
 491 mean task dissimilarity correlation for each value of α across all simulations. Bars indicate 95% confidence
 492 intervals across 25 simulations. This is shown separately for each Hidden layer of the two Hidden layer
 493 network in (a-b) and for the three Hidden layer network (c-e). The lower two rows (f-j) illustrate the
 494 distribution of activation at each Hidden layer of the two-layer network (f-g) and the three-layer network (h-
 495 j).

496 3.5. The location of modulation

497 To gain insight in how network performance is influenced by the location of modulation we
 498 performed additional simulations of the two Hidden layer network on the MNIST dataset. Here, we
 499 explored performance when the network received no modulatory input from the Task layer, when
 500 modulation was applied at the first Hidden layer (as before), at the second Hidden layer, or at both

501 Hidden layers. As can be observed in Figure 10a, all networks perform at chance level when no
 502 modulation is applied. When modulation is applied at one or more Hidden layers, the multiplicative
 503 modulating networks, and in particular the Ax network, outperforms the additive networks. Although
 504 network performance seems more reliable (narrow confidence intervals) with modulation at deeper
 505 and/or more Hidden layers, the increase in mean accuracy is very small.

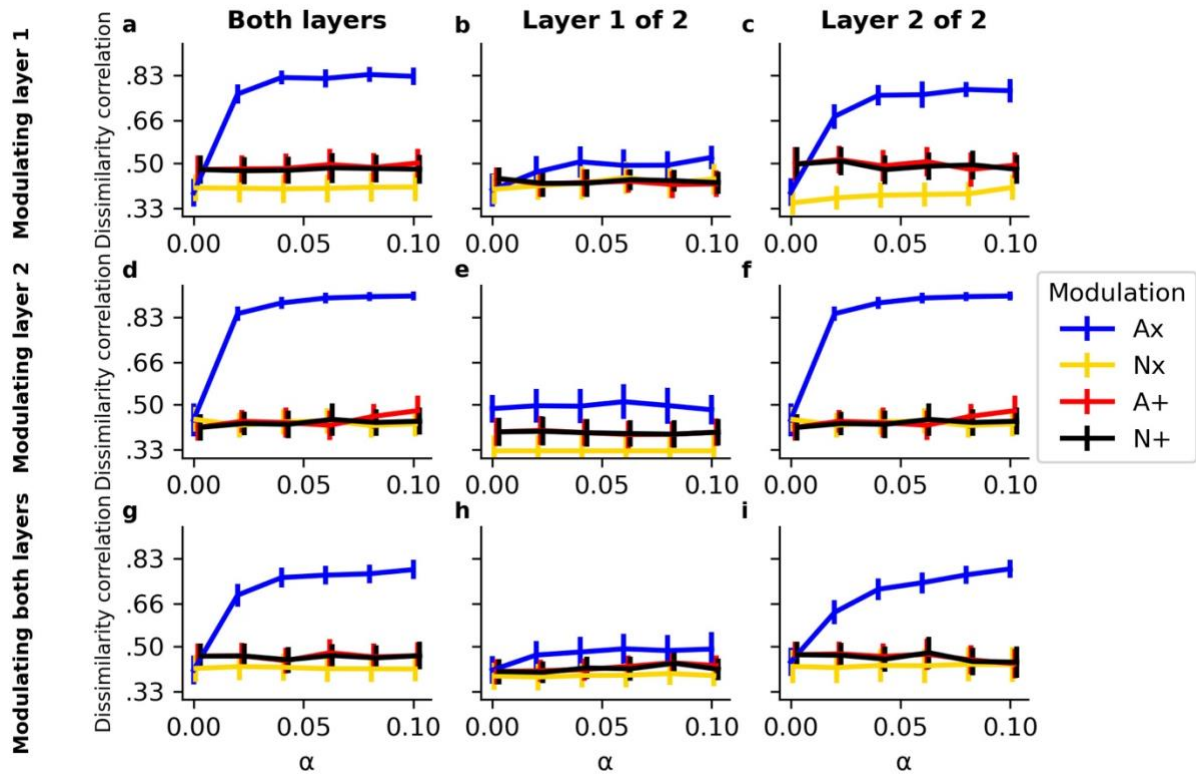


506

507 **Figure 10. Accuracy in test phase for different locations of modulation.** Lines illustrate mean accuracy
 508 during the test phase for each value of α , averaged across all tasks and all simulations. Bars indicate 95%
 509 confidence intervals over 25 simulations. The dashed lightgrey line indicates chance level accuracy. Results
 510 are shown for different datasets (rows) and different shapes of Hidden layer (columns).

511 Also the results of task representational dissimilarity correlations seem highly similar for all
 512 locations of modulation. Note that this analysis could not be performed for the network that used no
 513 modulation. Since there was no task modulation, task representations were completely similar and the
 514 representational dissimilarity matrices for these networks were constant. Hence, no correlation could
 515 be computed with the objective dissimilarity matrix.

516 In sum, there does not seem to be a significant difference in network performance depending
 517 on where modulation is applied. In this specific case, modulation at layer 2 could be considered as most
 518 optimal since it requires to only learn 100 weights from each Task neuron to that second layer, compared
 519 to 300 for the first layer, and 400 for both layers.



520

521 **Figure 11. Correlation of objective and representational dissimilarity depending on location of**
 522 **modulation.** Lines illustrate the mean task dissimilarity correlation for each value of α across all
 523 simulations. Bars indicate 95% confidence intervals over 25 simulations. Results are shown for different
 524 locations of modulation (rows) and different Hidden layer(s) (columns).

525

4. Discussion

526

527

528

529

530

531

532

Current work investigated how neural networks can optimally balance the trade-off between avoiding interference via separating task representations and generalizing information via sharing representations. For this purpose, we identified and systematically investigated two crucial features of modulation signals. First, the modulation signals can be additive or multiplicative. Multiplicative signals were better suited for separating task representations. The multiplicative networks were less vulnerable to catastrophic interference than the additive networks. Second, the modulation signals could be adaptive (learned) or non-adaptive (random). Adaptive modulation signals provided a clear

533 advantage over non-adaptive modulation signals in terms of both accuracy and balancing
534 representations. Hence, the adaptive multiplicative (Ax) network was able to optimally balance the
535 trade-off between sharing and separating task representations. This Ax network can avoid interference
536 but also generalize across tasks which resulted in an overall better accuracy compared to the other
537 networks.

538 Crucially, multiplicative signals modulated task-specific input more strongly. A Hidden
539 neuron that receives input from many bottom-up Stimulus neurons, needs a strong (negative) additive
540 modulation signal in order to be inhibited. In contrast, our multiplicative signal followed a RELU
541 activation function (Equation (4); see Supplementary materials for an investigation of activation
542 functions), which means that a small negative weight was sufficient to shut down (multiply by zero) a
543 Hidden neuron activation. As a result, multiplicative signals developed sparser representations (Figure
544 7) which is optimal for separating task representations. This advantage was especially present when
545 there were many Stimulus neurons (i.e., the MNIST task). When there were only 2 Stimulus neurons,
546 as in the Trees task (see Figure 1c), the additive network was also able to separate task representations
547 (see Figure 8h,k). Thus, multiplicative modulation is more efficient than additive signals, especially for
548 separating high-dimensional inputs. Specifically, the Ax network warped the representational space in
549 order to effectively organize tasks that obey similar mappings as well as tasks that obey dissimilar
550 mappings within one neural architecture. In this representational space, dissimilar tasks were placed at
551 the edges of a regular grid (see Figure 8c) and tasks that were similar were placed closer together. Such
552 a geometrical organization of task rules is optimally suited for generalizing task rules (Bernardi et al.,
553 2020; Kim, Pitt, & Myung, 2013). Consistent with the current analysis, Kim et al., (2013) demonstrated
554 how backpropagation shapes hidden space to accommodate quasi-regularities in language processing,
555 thus to accommodate both regular and irregular stimuli (e.g., orthography-phonology mappings). They
556 demonstrated that after training by backpropagation, both regular and irregular stimuli could be placed
557 in hidden neuron space at the edges of a slightly deformed grid; sufficiently grid-like to process the
558 regular stimuli (and profit from generalization), but sufficiently deformed to cope with irregular
559 mappings as well. Moreover, previous work has illustrated a similar systematicity of task

560 representations in neural activation of prefrontal areas and hippocampus of monkeys (Bernardi et al.,
561 2020).

562 An extensive amount of work describes how humans share or separate representations by
563 extracting latent states in the environment (Collins & Frank, 2016; Franklin & Frank, 2018; Gershman
564 & Niv, 2012; Wilson, Takahashi, Schoenbaum, & Niv, 2014; Yu, Wilson, & Nassar, 2020). Here, the
565 agent decides on every new experience whether to categorize it as belonging to a new state or as
566 belonging to a state that it has experienced before. Each latent state would then develop its own
567 representations. An important disadvantage of the latent state approach is that it uses a dichotomous
568 decision on whether an object belongs to the state or not. Such an approach is less suited to capture
569 partial overlap between tasks. In the example of the Stroop dataset, a latent state approach would
570 correctly assign tasks A, B and C to three different states because the mappings are completely
571 dissimilar. The latent state approach would also correctly assign task E to the same latent state as A
572 because they fully share the stimulus-action mappings. However, task D shares 1/3 of the mappings
573 with all four other tasks. In this case, D would be optimally handled as a combination of the other
574 mappings that are already learned. This is problematic for a latent state approach since it can only decide
575 to assign D to a new latent state or to one of the previous ones.

576 To accommodate this limitation of the latent state approach, previous work has proposed
577 compositionality (Fidler et al., 2009; Franklin & Frank, 2018; Lake et al., 2014; Sugita et al., 2011;
578 Tubiana & Monasson, 2017; Yang et al., 2019). Specifically, the latent state approach could allow
579 mixed overlap between tasks by representing a task as multiple states, each representing a subset of
580 mappings (Franklin & Frank, 2020; Griffiths & Ghahramani, 2011). Nevertheless, this approach could
581 significantly increase the number of possible states, which can be problematic in very complex task
582 environments. This raises the question in how many states/dimensions the agent should cluster its
583 experiences in order to optimally balance generalization and interference (Badre, Bhandari, Keglovits,
584 & Kikumoto, 2021). As we have shown in Figure 4a,b, the current Ax network could benefit equally
585 from the partial overlap in D and the full overlap between A and E without the need of extracting latent
586 states. This is consistent with previous work, showing that multiplicative network interactions lead to
587 useful compositional task representations (İrsoy & Cardie, 2015; Sugita et al., 2011).

588 Multiplicative modulation is also sometimes called gating (Masse et al., 2018; O'Reilly &
589 Frank, 2006; Rougier, Noelle, Braver, Cohen, & O'Reilly, 2005). A crucial question that remains is
590 how multiplicative signals are mechanistically implemented in the human brain. In this respect, we
591 point to recent work that described an important role for neural oscillations in organizing functional
592 networks. For example, it has been proposed that neural oscillations at alpha frequency (8-12 Hz) reflect
593 gating by inhibition (Jensen & Mazaheri, 2010). Here, GABAergic inhibition provided by the task-
594 irrelevant areas would be reflected by stronger alpha activity in those areas. Another oscillatory
595 frequency that is known to organize functional networks in the brain is the theta frequency (4-8 Hz).
596 More specifically, recent theoretical and empirical work (Helfrich & Knight, 2016; Lisman & Jensen,
597 2013; Verbeke et al., 2021; Verbeke & Verguts, 2019; Verguts, 2017) has proposed that prefrontal theta
598 activity functions to (de)synchronize gamma (>40 Hz) activity in posterior processing areas. Here,
599 synchronization leads to effective communication (gates open) between processing areas while
600 desynchronization eliminates effective communication (gates closed) between processing areas (Fries,
601 2005, 2015). Thus, previous work has described how oscillatory interactions within and between
602 different frequency bands (theta, alpha and gamma) reflect gating processes that could biologically
603 implement the multiplicative modulation signals that were used in the current networks.

604 Previous work has also described how neurotransmitters such as dopamine and noradrenaline
605 can modulate neural activation in a way that mimics multiplicative modulation (O'Reilly & Frank,
606 2006; Servan-Schreiber, Printz, & Cohen, 1990). Moreover, current work observed that additive
607 modulation can reach similar performance as multiplicative modulation when stimulus dimensionality
608 was low (Trees dataset). Hence, combining additive modulation with weight regularization between
609 Stimulus and Hidden layer but not between Task and Hidden layer could allow the additive modulation
610 networks to overcome high-dimensional inputs and reach similar performance as the multiplicative
611 modulation networks. Future work should further explore biologically plausible implementations of
612 multiplicative modulation.

613 In analogy to previous work (e.g., Cohen et al., 1990), the current networks used a low-
614 dimensional Task layer which sent modulation signals to modulate a higher-dimensional Hidden layer.
615 Typically, information in the Task layer has been considered to correspond to dorsolateral prefrontal

616 cortex (DLPFC) and the Hidden layer to posterior task-related (e.g., visual and motor) processing
617 pathways (Miller & Cohen, 2001). Hence, we propose that modulation signals are implemented by
618 DLPFC.

619 A detailed investigation of activation at Hidden layer (Figure 7) illustrated that
620 (multiplicative) networks separate tasks by developing sparse representations (see also Bowers,
621 Vankov, Damian, & Davis, 2014). Here, for every task, only a small subset of neurons is active. In the
622 current context, this suggests that the network develops groups or modules of neurons that each become
623 specialized for a given task. Developing specialized modules might be beneficial for cognition in
624 various ways (Bullinaria, 2007; Clune, Mouret, & Lipson, 2013; Coltheart, 1999; Fodor, 1983;
625 Meunier, Lambiotte, Fornito, Ersche, & Bullmore, 2009). Moreover, recent work in reinforcement
626 learning has also described hierarchical forms of modularity (Botvinick, Niv, & Barto, 2009; Dietterich,
627 2000; Holroyd & Verguts, 2021; Krueger & Dayan, 2009). Here, it is proposed that the dorsal part of
628 the anterior cingulate cortex processes prediction errors related to specific events while the rostral part
629 processes prediction errors related to the context in which these events occur (Alexander & Brown,
630 2015). However, modularity of processes in a single task requires integration of information across
631 stages of processing. Hence, exploring the trade-off between sharing and separating representations at
632 different levels of processing is an important avenue for future research.

633 In the current work, modulation signals are employed to guide learning over trials. Here, (for
634 the adaptive networks) weights between the Task and Hidden layer are adapted to learn representations
635 of different tasks. In contrast, a lot of previous work considered how modulation is adapted to guide
636 online performance. Here, the intensity of the modulation signal is typically increased in response to
637 some evaluation of the cost-benefit structure of the task context (Shenhav, Botvinick, & Cohen, 2013).
638 These networks typically adapt the intensity of the modulation signal by changing activity in the Task
639 layer instead of changing the weights (Botvinick et al., 2001; Verbeke & Verguts, 2020; Verguts, 2017).
640 Consistent with this approach, research on visual attention has proposed that activity can be modulated
641 (in a multiplicative manner) at the level of the Stimulus layer (Martinez-Trujillo & Treue, 2004; Treue
642 & Martínez Trujillo, 1999). Alternatively, previous work (Cheadle et al., 2014) suggested that decisions
643 can be guided via adaptive (multiplicative) gain functions in the transfer from input to output. Hence,

644 there is a potentially important functional distinction between modulation in learning versus
645 performance (see also Lindsay & Miller, 2017).

646 The trade-off between shared and separated representation also impacts performance
647 (Musslick et al., 2020) Specifically, a wide range of empirical observations of interference during multi-
648 tasking (performing multiple tasks at the same time) can be explained by a tendency to share task
649 representations. Musslick et al. (2020) suggest that for generalization purposes, representations of novel
650 tasks should strongly overlap with other task representations; unfortunately, such overlap leads to strong
651 interference when these tasks need to be performed at the same time. However, with extensive training,
652 the networks will gradually separate task representations, which leads to less interference. Hence, future
653 work should consider a more extensive exploration of modulation signals in performance as well.

654 We evaluated the ability of different modulation signals to balance shared and separated
655 representations by investigating how the networks could overcome catastrophic interference.
656 Importantly, while modulation has proven to be efficient (Masse et al., 2018; Verbeke & Verguts, 2019),
657 previous work also described other methods to avoid catastrophic interference. For instance, sharing or
658 separation of task sets might be implemented in complementary learning systems (O'Reilly & Norman,
659 2002). Alternatively, machine learning literature has introduced methods such as synaptic intelligence
660 (Kirkpatrick et al., 2017) in which weights learn whether they should be specific for one task and hence
661 not change during further learning or whether they can be shared across all tasks. Future work should
662 further address the differences between these approaches.

663 Several additional tests and extensions can be made to the network. First, previous work
664 (Flesch et al., 2018) has pointed to an important distinction between interference in artificial and human
665 agents. While artificial agents show more interference when they learn in a blocked fashion, human
666 agents exhibit more interference when they learn in an interleaved fashion. The current work trained
667 artificial agents in a blocked fashion. However, the different types of modulation signals should also be
668 evaluated for interleaved learning. Potentially this approach could yield more insight in the existing
669 distinction of learning benefits for artificial compared to human agents. Second, the current networks
670 did not learn which task features were relevant for modulation. Here, the input layer was divided a-
671 priori in a Stimulus group and a Task group. Hence, an important next step for the network would be to

672 learn a hierarchical structure in input features in order to extract which inputs are relevant for
673 modulation and which are relevant for basic stimulus-action mappings (Rougier et al., 2005).
674 Alternatively, previous work has illustrated that compositional representations can even develop
675 without providing task input if they are considered useful as situational signals (Butz et al., 2021). Third,
676 although we illustrated that the Ax network was able to significantly benefit (in terms of accuracy) from
677 shared mappings between tasks (Figure 4a,b), we did not perform a direct test of generalization. That
678 is, we did not evaluate whether newly learned mappings in Task A of the Stroop task were transferred
679 to task E without further training in task E. That is, we did not test whether the learned task relations
680 were also suited for few-shot learning (Lake et al., 2014; Sylvain, Petrini, & Hjelm, 2020). Note that
681 for an exact transfer between A and E, the weight matrix between Task neuron A and the Hidden layer
682 should be exactly the same as the weight matrix between Task neuron E and the Hidden layer, which
683 seems a strong requirement. Yet, it is not clear either whether two contexts that require the same
684 stimulus-action mappings would also function in exactly the same way at behavioral and neural levels.
685 Nor is this computationally desirable: In the natural environment, two labels that lead to the same
686 stimulus-action contingencies, may still suggest (subtle) differences. Consider looking for lunch and
687 seeing a “restaurant” versus a “snack bar” in the distance: Both tell you that you will be able to eat
688 there, but expectations will differ at least slightly. As we discussed before, extracting a relational
689 structure between contexts that allows for partial generalization might be more optimal than using a
690 dichotomous same or different decision.

691 In sum, efficient human learning and performance requires to balance a trade-off between
692 sharing representations to allow generalization and separating representations to avoid interference. We
693 evaluated four different modulation signals and found that an adaptive multiplicative modulation signal
694 was best suited to balance the sharing/separation trade-off. This modulation signal allowed the Hidden
695 layer of the network to make a geometrical abstraction of the relational structure between tasks.
696 Importantly, our work opens several avenues for future work to increase the understanding of the
697 sharing/separation trade-off in both artificial and human agents.

698

699

5. References

- 700 Aben, B., Calderon, C. B., Van den Bussche, E., & Verguts, T. (2020). Cognitive Effort Modulates
701 Connectivity between Dorsal Anterior Cingulate Cortex and Task-Relevant Cortical Areas. *The*
702 *Journal of Neuroscience*, *40*(19). <https://doi.org/10.1523/jneurosci.2948-19.2020>
- 703 Abrahamse, E., Braem, S., Notebaert, W., & Verguts, T. (2016). Grounding Cognitive Control in
704 Associative Learning. *Psychological Bulletin*, *142*(7), 693–728.
705 <https://doi.org/10.1037/bul0000047>
- 706 Alexander, W. H., & Brown, J. W. (2015). Hierarchical error representation: A computational model
707 of anterior cingulate and dorsolateral prefrontal cortex. *Neural Computation*, *27*(11), 2354–
708 2410. <https://doi.org/10.1162/NECO>
- 709 Alon, N., Reichman, D., Shinkar, I., Wagner, T., Musslick, S., Cohen, J. D., ... Ozcimder, K. (2017).
710 A graph-theoretic approach to multitasking. In *Advances in Neural Information Processing*
711 *Systems* (pp. 2097–2106).
- 712 Badre, D., Bhandari, A., Keglovits, H., & Kikumoto, A. (2021). The dimensionality of neural
713 representations for control. *Current Opinion in Behavioral Sciences*, *38*, 20–28.
714 <https://doi.org/10.1016/j.cobeha.2020.07.002>
- 715 Baxter, J. (2019). Learning Internal Representations. In *Proceedings of the eighth annual conference*
716 *on computational learning theory* (pp. 311–320).
717 <https://doi.org/10.7551/mitpress/2906.003.0006>
- 718 Bernardi, S., Benna, M. K., Rigotti, M., Munuera, J., Fusi, S., & Salzman, C. D. (2020). The
719 Geometry of Abstraction in the Hippocampus and Prefrontal Cortex. *Cell*, *183*(4), 954–967.
720 <https://doi.org/10.1016/j.cell.2020.09.031>
- 721 Botvinick, M. M., Braver, T. S., Barch, D. M., Carter, C. S., & Cohen, J. D. (2001). Conflict
722 monitoring and cognitive control. *Psychological Review*, *108*(3), 624–652.
723 <https://doi.org/10.1037/0033-295X.108.3.624>
- 724 Botvinick, M. M., Niv, Y., & Barto, A. C. (2009). Hierarchically organized behavior and its neural
725 foundations : A reinforcement learning perspective. *Cognition*, *113*(3), 262–280.
726 <https://doi.org/10.1016/j.cognition.2008.08.011>
- 727 Bouchacourt, F., & Buschman, T. J. (2019). A Flexible Model of Working Memory. *Neuron*, *103*(1),

- 728 147–160. <https://doi.org/10.1016/j.neuron.2019.04.020>
- 729 Bowers, J. S., Vankov, I. I., Damian, M. F., & Davis, C. J. (2014). Neural networks learn highly
730 selective representations in order to overcome the superposition catastrophe. *Psychological*
731 *Review*, *121*(2), 248–261. <https://doi.org/10.1037/a0035943>
- 732 Bullinaria, J. A. (2007). Understanding the advantage of modularity in neural systems. *Cognitive*
733 *Science*, *31*(4), 673–695. <https://doi.org/10.1080/15326900701399939>
- 734 Butz, M. V., Achimova, A., Bilkey, D., & Knott, A. (2021). Event-Predictive Cognition: A Root for
735 Conceptual Human Thought. *Topics in Cognitive Science*, *13*(1), 10–24.
736 <https://doi.org/10.1111/tops.12522>
- 737 Butz, M. V., Bilkey, D., Humaidan, D., Knott, A., & Otte, S. (2019). Learning, planning, and control
738 in a monolithic neural event inference architecture. *Neural Networks*, *117*, 135–144.
739 <https://doi.org/10.1016/j.neunet.2019.05.001>
- 740 Cheadle, S., Wyart, V., Tsetsos, K., Myers, N., deGardelle, V., HerceCastañón, S., & Summerfield, C.
741 (2014). Adaptive gain control during human perceptual choice. *Neuron*, *81*(6), 1429–1441.
742 <https://doi.org/10.1016/j.neuron.2014.01.020>
- 743 Clune, J., Mouret, J. B., & Lipson, H. (2013). The evolutionary origins of modularity. *Proceedings of*
744 *the Royal Society B: Biological Sciences*, *280*(1755). <https://doi.org/10.1098/rspb.2012.2863>
- 745 Cohen, J. D., Dunbar, K., & McClelland, J. L. (1990). On the control of automatic processes: a
746 parallel distributed processing account of the Stroop effect. *Psychological Review*, *97*(3), 332–
747 361. <https://doi.org/10.1037/0033-295X.97.3.332>
- 748 Collins, A. G. E., & Frank, M. J. (2016). Neural signature of hierarchically structured expectations
749 predicts clustering and transfer of rule sets in reinforcement learning. *Cognition*, *152*, 160–169.
750 <https://doi.org/10.1016/j.cognition.2016.04.002>
- 751 Coltheart, M. (1999). Modularity and cognition. *Trends in Cognitive Sciences*, *3*(3), 115–120.
752 [https://doi.org/10.1016/S1364-6613\(99\)01289-9](https://doi.org/10.1016/S1364-6613(99)01289-9)
- 753 Dietterich, T. G. (2000). Hierarchical reinforcement learning with the MAXQ value function
754 decomposition. *Journal of Artificial Intelligence Research*, *13*, 227–303.
755 <https://doi.org/10.1613/jair.639>

- 756 Fidler, S., Boben, M., & Leonardis, A. (2009). Learning hierarchical compositional representations of
757 object structure. *Object Categorization: Computer and Human Vision Perspectives*,
758 9780521887, 196–215. <https://doi.org/10.1017/CBO9780511635465.012>
- 759 Flesch, T., Balaguer, J., Dekker, R., Nili, H., & Summerfield, C. (2018). Comparing continual task
760 learning in minds and machines. *Proceedings of the National Academy of Sciences of the United*
761 *States of America*, 115(44). <https://doi.org/10.1073/pnas.1800755115>
- 762 Fodor, J. A. (1983). *The modularity of mind*. MIT Press/Bradford Books.
- 763 Franklin, N. T., & Frank, M. J. (2018). Compositional clustering in task structure learning. *PLoS*
764 *Computational Biology*, 14(4), 1–25. <https://doi.org/10.1371/journal.pcbi.1006116>
- 765 Franklin, N. T., & Frank, M. J. (2020). Generalizing to generalize: Humans flexibly switch between
766 compositional and conjunctive structures during reinforcement learning. *PLoS Computational*
767 *Biology*, 16(4), 1–33. <https://doi.org/10.1371/journal.pcbi.1007720>
- 768 French, R. M. (1999). Catastrophic forgetting in connectionist networks. *Trends in Cognitive*
769 *Sciences*, 3(4), 128–135.
- 770 Fries, P. (2005). A mechanism for cognitive dynamics: neuronal communication through neuronal
771 coherence. *Trends in Cognitive Sciences*, 9(10), 474–480.
772 <https://doi.org/10.1016/j.tics.2005.08.011>
- 773 Fries, P. (2015). Rhythms for Cognition: Communication through Coherence. *Neuron*, 88(1), 220–
774 235. <https://doi.org/10.1016/j.neuron.2015.09.034>
- 775 Gershman, S. J., & Niv, Y. (2012). Exploring a latent cause theory of classical conditioning. *Learning*
776 *and Behavior*, 40(3), 255–268. <https://doi.org/10.3758/s13420-012-0080-8>
- 777 Griffiths, T. L., & Ghahramani, Z. (2011). The Indian buffet process: An introduction and review.
778 *Journal of Machine Learning Research*, 12, 1185–1224.
- 779 Helfrich, R. F., & Knight, R. T. (2016). Oscillatory Dynamics of Prefrontal Cognitive Control. *Trends*
780 *in Cognitive Sciences*, 20(12), 916–930. <https://doi.org/10.1016/j.tics.2016.09.007>
- 781 Holroyd, C. B., & Verguts, T. (2021). The best laid plans: Computational principles of ACC. *Trends*
782 *in Cognitive Sciences*, 25(4), 316–329. <https://doi.org/10.1016/j.tics.2021.01.008>
- 783 Hupkes, D., Dankers, V., Mul, M., & Bruni, E. (2020). Compositionality decomposed: How do neural

- 784 networks generalise? *Journal of Artificial Intelligence Research*, 67, 757–795.
- 785 Irsoy, O., & Cardie, C. (2014). Deep recursive neural networks for compositionality in language.
786 *Advances in Neural Information Processing Systems*, 3(January), 2096–2104.
- 787 Irsoy, O., & Cardie, C. (2015). Modeling compositionality with multiplicative recurrent neural
788 networks. *3rd International Conference on Learning Representations, ICLR 2015 - Conference*
789 *Track Proceedings*, (2013), 1–10.
- 790 Jensen, O., & Mazaheri, A. (2010). Shaping functional architecture by oscillatory alpha activity:
791 Gating by inhibition. *Frontiers in Human Neuroscience*, 4, 1–8.
792 <https://doi.org/10.3389/fnhum.2010.00186>
- 793 Kim, W., Pitt, M. A., & Myung, J. I. (2013). How Do PDP Models Learn Quasiregularity?
794 *Psychological Review*, 120(4), 903–916. <https://doi.org/10.1037/a0034195>
- 795 Kirkpatrick, J., Pascanu, R., Rabinowitz, N., Veness, J., Desjardins, G., Rusu, A. A., ... Hadsell, R.
796 (2017). Overcoming Catastrophic Forgetting in Neural Networks. *Proceedings of the National*
797 *Academy of Sciences*, 114(13), 3521–3526. <https://doi.org/10.1073/pnas.1611835114>
- 798 Krueger, K. A., & Dayan, P. (2009). Flexible shaping: How learning in small steps helps. *Cognition*,
799 110(3), 380–394. <https://doi.org/10.1016/j.cognition.2008.11.014>
- 800 Lake, B., & Baroni, M. (2018). Generalization without systematicity: On the compositional skills of
801 sequence-to-sequence recurrent networks. *35th International Conference on Machine Learning*,
802 *ICML 2018*, 7, 4487–4499.
- 803 Lake, B., Lee, C.-Y., Glass, J., Lake, B. M., Glass, J. R., & Tenenbaum, J. B. (2014). One-shot
804 learning of generative speech concepts Publication Date One-shot learning of generative speech
805 concepts. *Proceedings of the Annual Meeting of the Cognitive Science Society*, (36), 803–808.
806 Retrieved from <https://cloudfront.escholarship.org/dist/prd/content/qt3xf2n3vc/qt3xf2n3vc.pdf>
- 807 Lake, B., Ullman, T., Tenenbaum, J., & Gershman, S. (2017). Building machines that learn and think
808 like people. *Behavioral and Brain Sciences*, 40(2017).
809 <https://doi.org/10.1017/S0140525X16001837>
- 810 LeCun, Y., Cortes, C., & Burges, C. J. (2010). MNIST handwritten digit database.
- 811 Lillicrap, T. P., Cownden, D., Tweed, D. B., & Akerman, C. J. (2016). Random synaptic feedback

- 812 weights support error backpropagation for deep learning. *Nature Communications*, 7, 1–10.
- 813 <https://doi.org/10.1038/ncomms13276>
- 814 Lindsay, G. W., & Miller, K. D. (2018). How biological attention mechanisms improve task
- 815 performance in a large-scale visual system model. *ELife*, 7, 1–29.
- 816 <https://doi.org/10.7554/eLife.38105.001>
- 817 Lisman, J. E., & Jensen, O. (2013). The Theta-Gamma Neural Code. *Neuron*, 77(6), 1002–1016.
- 818 <https://doi.org/10.1016/j.neuron.2013.03.007>
- 819 Maass, W., Natschläger, T., & Markram, H. (2002). Real-time computing without stable states: A
- 820 new framework for neural computation based on perturbations. *Neural Computation*, 14(11),
- 821 2531–2560. <https://doi.org/10.1162/089976602760407955>
- 822 Martinez-Trujillo, J. C., & Treue, S. (2004). Feature-Based Attention Increases the Selectivity of
- 823 Population Responses in Primate Visual Cortex. *Current Biology*, 14, 744–751.
- 824 <https://doi.org/10.1016/j.cub.2004.04.028>
- 825 Masse, N. Y., Grant, G. D., & Freedman, D. J. (2018). Alleviating catastrophic forgetting using
- 826 context-dependent gating and synaptic stabilization. *Proceedings of the National Academy of*
- 827 *Sciences*, 115(44), 1–12. <https://doi.org/10.1073/pnas.1803839115>
- 828 McClelland, J. L., McNaughton, B. L., & O'Reilly, R. C. (1995). Why There Are Complementary
- 829 Learning Systems in the Hippocampus and Neo-cortex: Insights from the Successes and Failures
- 830 of Connectionists Models of Learning and Memory. *Psychological Review.*, 102(3), 419–457.
- 831 <https://doi.org/10.1037/0033-295X.102.3.419>
- 832 Meunier, D., Lambiotte, R., Fornito, A., Ersche, K. D., & Bullmore, E. T. (2009). Hierarchical
- 833 modularity in human brain functional networks. *Frontiers in Neuroinformatics*, 3, 1–12.
- 834 <https://doi.org/10.3389/neuro.11.037.2009>
- 835 Miller, E. K., & Cohen, J. D. (2001). An Integrative Theory of Prefrontal Cortex Function. *Annual*
- 836 *Review of Neuroscience*, 24, 167–202. <https://doi.org/10.1146/annurev.neuro.24.1.167>
- 837 Musslick, S., & Cohen, J. D. (2020). Rationalizing constraints on the capacity for cognitive control.
- 838 *PsyArxiv*, 45. <https://doi.org/10.31234/osf.io/vtknh>
- 839 Musslick, S., Saxe, A. M., Ozcimder, K., Dey, B., Henselman, G., & Cohen, J. D. (2017).

- 840 Multitasking Capability Versus Learning Efficiency in Neural Network Architectures. In *Annual*
841 *meeting of the Cognitive Science Society* (pp. 829–834).
- 842 Musslick, S., Saxe, A., Novick, A., Reichman, D., & Cohen, J. D. (2020). On the rational
843 boundedness of cognitive control: Shared versus separated representations. *PsyArXiv*.
844 <https://doi.org/10.31234/osf.io/jkhdf>
- 845 O'Reilly, R. C., & Frank, M. J. (2006). Making Working Memory Work : A Computational Model of
846 Learning in the Prefrontal Cortex and Basal Ganglia. *Neural Computation*, *18*(2), 283–328.
847 <https://doi.org/10.1162/089976606775093909>
- 848 O'Reilly, R. C., & Norman, K. A. (2002). Hippocampal and neocortical contributions to memory:
849 Advances in the complementary learning systems framework. *Trends in Cognitive Sciences*,
850 *6*(12), 505–510. [https://doi.org/10.1016/S1364-6613\(02\)02005-3](https://doi.org/10.1016/S1364-6613(02)02005-3)
- 851 Rougier, N. P., Noelle, D. C., Braver, T. S., Cohen, J. D., & O'Reilly, R. C. (2005). Prefrontal cortex
852 and flexible cognitive control: Rules without symbols. *Proceedings of the National Academy of*
853 *Sciences of the United States of America*, *102*(20), 7338–7343.
854 <https://doi.org/10.1073/pnas.0502455102>
- 855 Rumelhart, D. E., Hinton, G. E., & Williams, R. J. (1986). Learning representations by back-
856 propagating errors. *Nature*, *323*, 533–536. <https://doi.org/10.1038/323533a0>
- 857 Sagiv, Y., Musslick, S., Niv, Y., & Cohen, J. D. (2020). Efficiency of learning vs. processing:
858 Towards a normative theory of multitasking. In *Proceedings of the 40th Annual Meeting of the*
859 *Cognitive Science Society*, (p. 1004—1009).
- 860 Servan-Schreiber, D., Printz, H., & Cohen, J. D. (1990). A network model of catecholamine effects:
861 Gain, signal-to-noise ratio, and behavior. *Science*, *249*(4971), 892–895.
862 <https://doi.org/10.1126/science.2392679>
- 863 Shenhav, A., Botvinick, M. M., & Cohen, J. D. (2013). The expected value of control: An integrative
864 theory of anterior cingulate cortex function. *Neuron*, *79*(2), 217–240.
865 <https://doi.org/10.1016/j.neuron.2013.07.007>
- 866 Stroop, J. R. (1935). Studies of interference in serial verbal reactions. *Journal of Experimental*
867 *Psychology*, *18*(6), 643–662. <https://doi.org/10.1037/h0054651>

- 868 Sugita, Y., Tani, J., & Butz, M. V. (2011). Simultaneously emerging braitenberg codes and
869 compositionality. *Adaptive Behavior*, *19*(5), 295–316.
870 <https://doi.org/10.1177/1059712311416871>
- 871 Sylvain, T., Petrini, L., & Hjelm, R. D. (2020). Zero-Shot Learning from scratch (ZFS): leveraging
872 local compositional representations. Retrieved from <http://arxiv.org/abs/2010.13320>
- 873 Treue, S., & Martínez Trujillo, J. C. (1999). Feature-based attention influences motion processing
874 gain in macaque visual cortex. *Nature*, *399*, 575–579. <https://doi.org/10.1038/21176>
- 875 Tsai, C. Y., Saxe, A., & Cox, D. (2016). Tensor switching networks. *Advances in Neural Information*
876 *Processing Systems*, (Nips), 2046–2054.
- 877 Tubiana, J., & Monasson, R. (2017). Emergence of Compositional Representations in Restricted
878 Boltzmann Machines. *Physical Review Letters*, *118*(13), 1–5.
879 <https://doi.org/10.1103/PhysRevLett.118.138301>
- 880 Vaidya, A. R., Jones, H. M., Castillo, J., & Badre, D. (2021). Neural representation of abstract task
881 structure during generalization. *ELife*, (10:e63226.), 1–22. <https://doi.org/10.7554/eLife.63226>
- 882 Verbeke, P., Ergo, K., De Loof, E., Verguts, T., Loof, E. De, & Verguts, T. (2021). Learning to
883 synchronize: Midfrontal theta dynamics during rule switching. *Journal of Neuroscience*, *41*(7),
884 1–13. <https://doi.org/10.1523/JNEUROSCI.1874-20.2020>
- 885 Verbeke, P., & Verguts, T. (2019). Learning to synchronize: How biological agents can couple neural
886 task modules for dealing with the stability-plasticity dilemma. *PLoS Computational Biology*,
887 *15*(8). <https://doi.org/10.1371/journal.pcbi.1006604>
- 888 Verbeke, P., & Verguts, T. (2020). Neural synchrony for adaptive control. *Psyarxiv*, 1–37.
889 <https://doi.org/10.31234/osf.io/523x9>
- 890 Verguts, T. (2017). Binding by random bursts: A computational model of cognitive control. *Journal*
891 *of Cognitive Neuroscience*, *29*(6), 1103–1118. <https://doi.org/10.1162/jocn>
- 892 Verguts, T., & Notebaert, W. (2008). Hebbian Learning of Cognitive Control : Dealing With Specific
893 and Nonspecific Adaptation. *Psychological Review*, *115*(2), 518–525.
894 <https://doi.org/10.1037/0033-295X.115.2.518>
- 895 Wilson, R. C., Takahashi, Y. K., Schoenbaum, G., & Niv, Y. (2014). Orbitofrontal cortex as a

- 896 cognitive map of task space. *Neuron*, 81(2), 267–279.
- 897 <https://doi.org/10.1016/j.neuron.2013.11.005>
- 898 Yang, G. R., Joglekar, M. R., Song, H. F., Newsome, W. T., & Wang, X. J. (2019). Task
- 899 representations in neural networks trained to perform many cognitive tasks. *Nature*
- 900 *Neuroscience*, 22(2), 297–306. <https://doi.org/10.1038/s41593-018-0310-2>
- 901 Yu, L. Q., Wilson, R. C., & Nassar, M. R. (2020). Adaptive learning is structure learning in time.
- 902 *Psyarxiv*, 1–27. <https://doi.org/10.31234/osf.io/r637c>
- 903 Zambaldi, V., Raposo, D., Santoro, A., Bapst, V., Li, Y., Babuschkin, I., ... Battaglia, P. (2018).
- 904 Relational Deep Reinforcement Learning, (2), 1–15. Retrieved from
- 905 <http://arxiv.org/abs/1806.01830>
- 906

Supplementary materials

S.1. Exploration of activation functions

In the main text (see Equation (2)), multiplicative modulation was established by combining two nonlinear transformations of the Stimulus and Task input via $f()$ and $g()$. Here, $f()$ represented the sigmoid activation function (see Equation (3)) and $g()$ represented a RELU activation function (see Equation (4)). Additive modulation (see Equation (1)) was implemented by transforming both the Task and Stimulus input with $f()$. Here, we present 4 novel simulations in which we explored all combinations of activation functions. Specifically, we tested networks in which both $f()$ and $g()$ corresponded to the sigmoid function (i.e. Sig (\otimes Sig)), we tested when $f()$ corresponded to the sigmoid function and $g()$ to the RELU function (i.e. Sig (\otimes RELU); as in the main text), we tested when $f()$ corresponded to the RELU function and $g()$ to the sigmoid function (i.e. RELU (\otimes Sig)) and we tested the networks when both $f()$ and $g()$ corresponded to the RELU function (i.e. RELU (\otimes RELU)). Note that for the additive modulation networks, only $f()$ is relevant. This is why our notation shows the second function (i.e., $g()$) between brackets.

For these additional simulations, the networks were tested on the Stroop and Trees dataset with 12 Hidden neurons. We again explored different values of α ranging from 0 to 1 in steps of .2. Again, 25 simulations were performed in which we shuffled task contexts and trained networks for three context repetitions after which weights were frozen and the networks were tested again on each context.

Accuracy and dissimilarity correlations were analysed during the test phase. As can be observed (Figure S1), the network that is presented in the main text Sig (\otimes RELU) is most optimal for both the multiplicative and additive modulation networks. Although the multiplicative modulation seemed less efficient when implemented via a sigmoid function (Figure S1a,c,e,g,i,k,m,o), the Ax network still outperformed the other modulation methods. Presumably, the RELU function is more efficient for modulation because it operates at a much larger scale $[0, +\infty]$ than the sigmoid function which has bounds at 0 and 1.

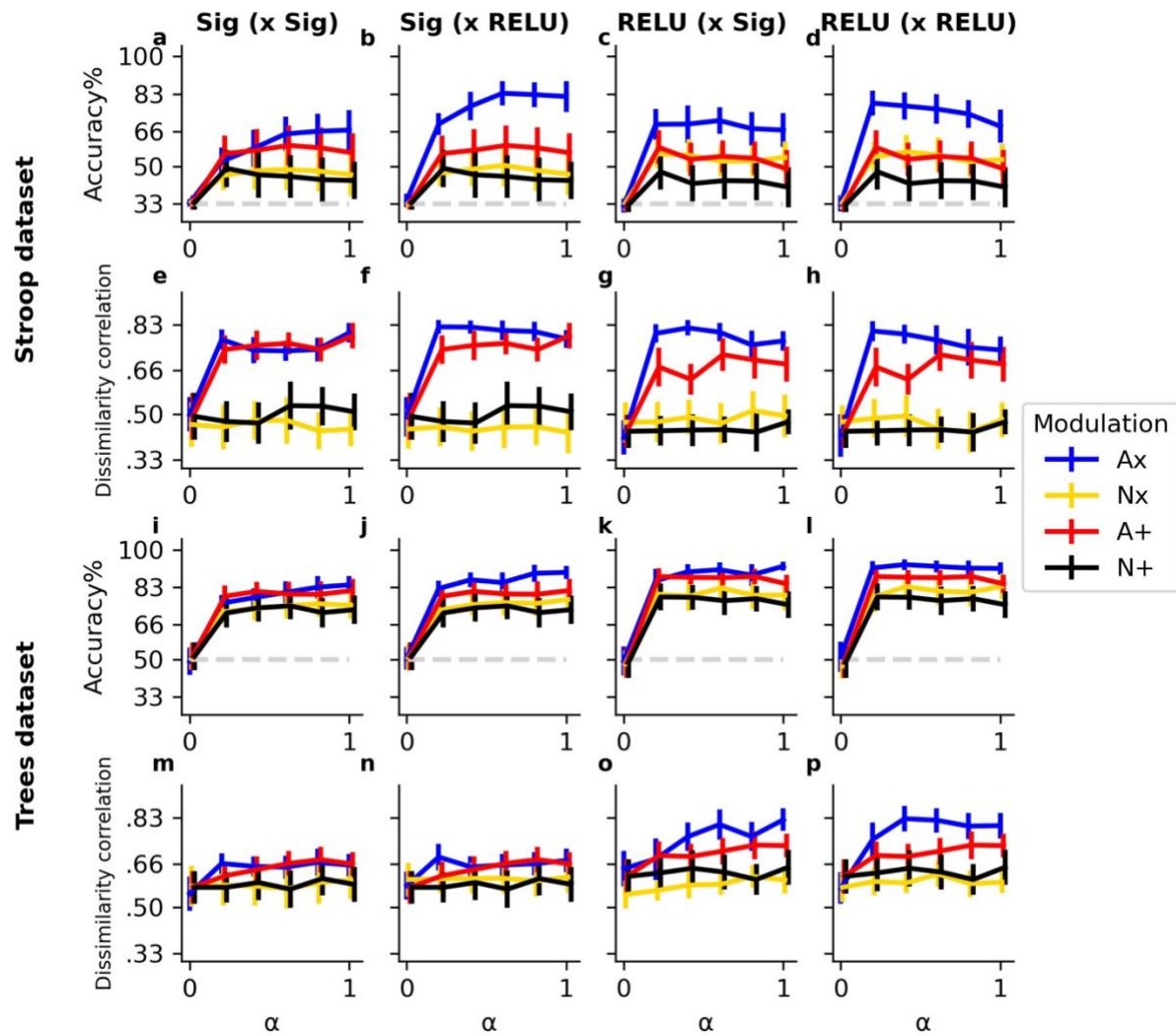


Figure S1. Activation function exploration. Lines illustrate mean accuracy/dissimilarity correlations for each value of α across all tasks and all simulations. Bars indicate 95% confidence intervals over 25 simulations. The dashed lightgrey line indicates chance level accuracy. Results are shown for different datasets (rows) and different combinations of activation functions (columns).

S.2. Concatenated versus separated input transformations

In the main text (see Equation (2)), multiplicative modulation was established by combining two separated nonlinear transformations of the Stimulus and Task input via $f(SW) \otimes g(TW)$ while Additive modulation (see Equation (1)) was implemented by transforming both the Task and Stimulus input with $f(SW+TW)$. Hence, for additive modulation, inputs were concatenated in one transformation, while for multiplicative modulation inputs were separated in two transformations. We choose these different implementations because they are most closely related to previous work (e.g., Cohen, Dunbar, & McClelland, 1990; Masse, Grant, & Freedman, 2018 for additive and multiplicative modulation

respectively). However, for completeness, we also explored other implementations of multiplicative and additive modulation. Specifically, we tested networks in which for both types of modulation (additive and multiplicative) the inputs were concatenated. This results in $f(SW) \otimes g(TW)$ for multiplicative modulation and $f(SW) + g(TW)$ for additive modulation. Additionally, we tested networks in which the inputs were separated. This resulted in $f(SW \otimes TW)$ for multiplicative modulation and $f(SW) + TW$ for additive modulation.

Again, the networks were tested on the Stroop and Trees dataset with 12 Hidden neurons. We explored different values of α going from 0 to 1 in steps of .2 and 25 simulations were performed in which we shuffled task contexts and trained networks for three context repetitions after which weights were frozen and the networks were tested again on each context.

Accuracy and dissimilarity correlations were analysed during the test phase. As illustrated in (Figure S2), for none of the modulation methods there is a clear difference when using separated versus concatenated input transformations.

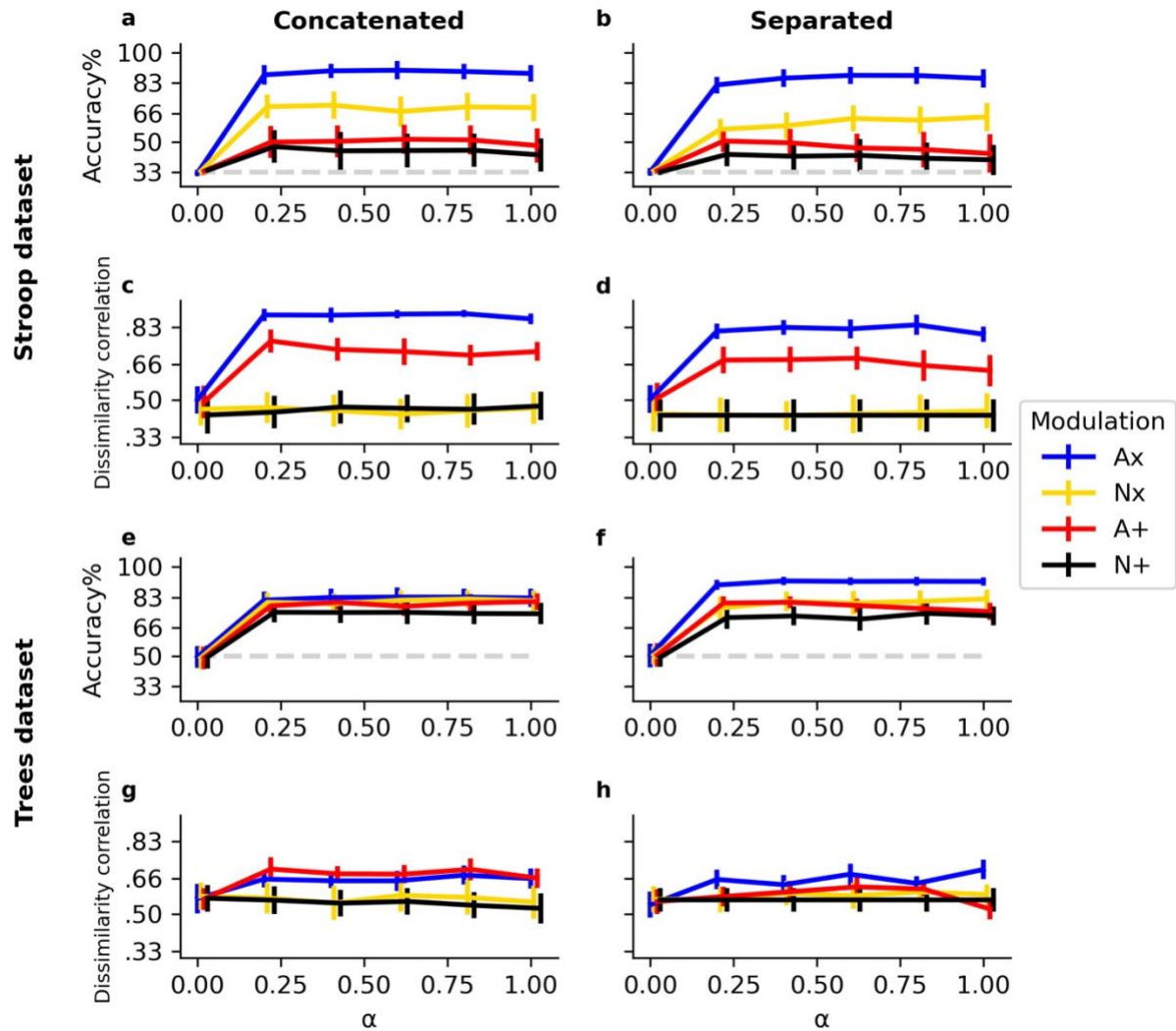


Figure S2. Concatenated versus separated input transformations. Lines illustrate mean accuracy/dissimilarity correlations for each value of α across all tasks and all simulations. Bars indicate 95% confidence intervals over 25 simulations. The dashed lightgrey line indicates chance level accuracy. Results are shown for different datasets (rows) and different concatenated versus separated input transformations (columns).

S.3. Exploration of weight initialization

In the main text we described that all weights are initialized with a random value drawn from the normal distribution $N(0, 1)$. Only for the Ax network, modulating weights (between Task and Hidden layer) had an initial random value drawn from the uniform distribution $U(0, 1)$, such that $\text{RELU}(\mathbf{T}) > 0$ (all gates open) at the first trial. However, previous work has demonstrated that the way in which weights are initialized is not trivial (e.g., Flesch, Juechems, Dumbalska, & Saxe, 2021). To illustrate that our results were not solely driven by this choice of weight initialization, we performed

additional simulations in which we tested a normal initialization for all modulating weights and compared this to a uniform initialization for all modulating weights.

The networks were again tested on the Stroop and Trees dataset with 12 Hidden neurons. We explored different values of α ranging from 0 to 1 in steps of .2. Again, 25 simulations were performed in which we shuffled task contexts and trained networks for three context repetitions after which weights were frozen and the networks were tested again on each context.

As shown in Figure S3, the Ax network indeed performs a bit worse when the weights are initialized from the normal distribution. However, it is also the case that for the other three networks the uniform initialization was a bit less optimal. Hence, the main text describes simulations in which the optimal weight initialization was chosen for each of the four modulation methods.

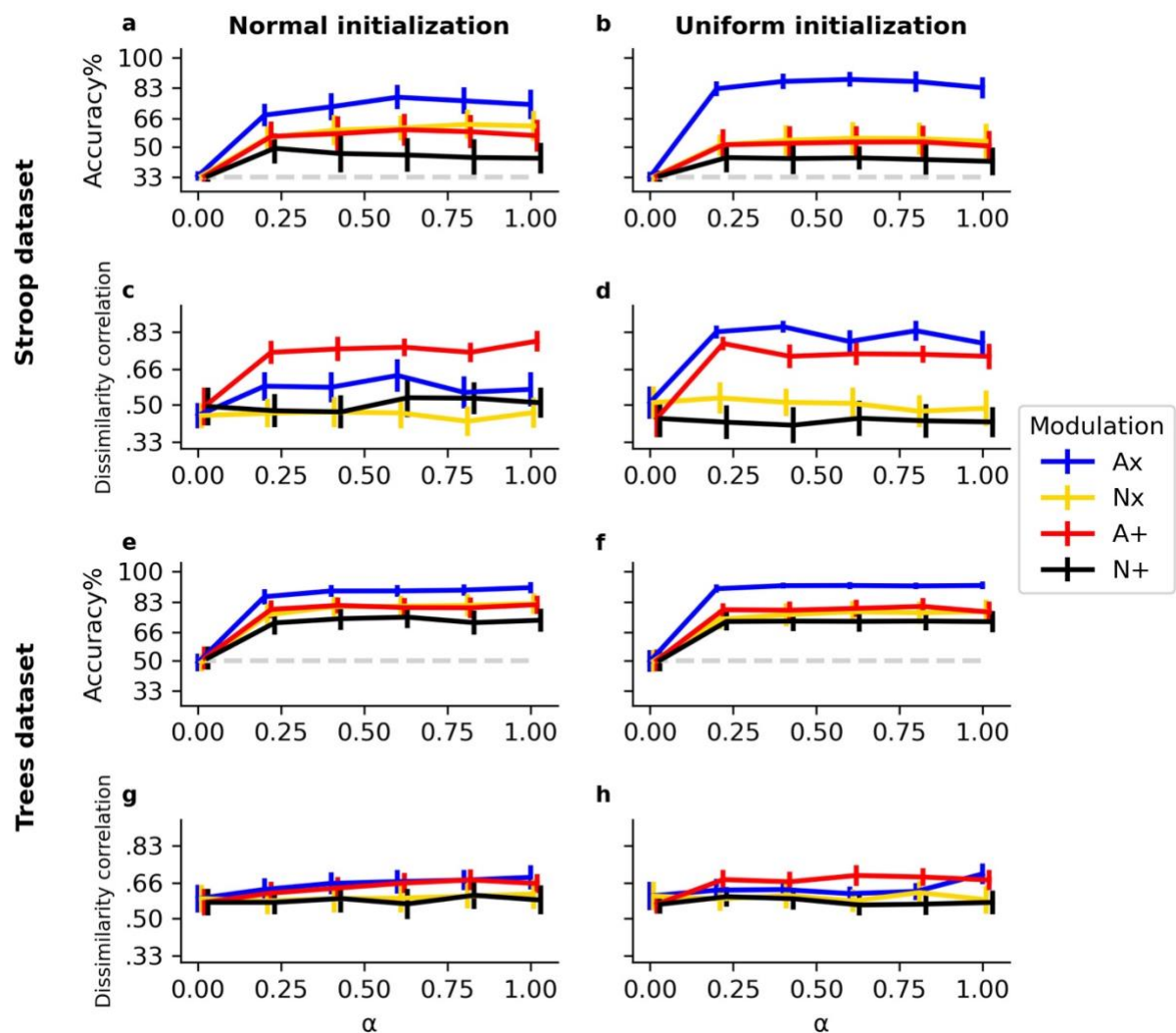


Figure S2. Weight initialization exploration. Lines illustrate mean accuracy/dissimilarity correlations for each value of α across all tasks and all simulations. Bars indicate 95% confidence intervals over 25 simulations. The dashed lightgrey line indicates chance level accuracy. Results are shown for different datasets (rows) and for different initializations of the modulation weights (columns).

References

- Cohen, J. D., Dunbar, K., & McClelland, J. L. (1990). On the control of automatic processes: a parallel distributed processing account of the Stroop effect. *Psychological Review*, *97*(3), 332–361. <https://doi.org/10.1037/0033-295X.97.3.332>
- Flesch, T., Juechems, K., Dumbalska, T., & Saxe, A. (2021). Rich and lazy learning of task representations in brains and neural networks. *BioRxiv*.
- Masse, N. Y., Grant, G. D., & Freedman, D. J. (2018). Alleviating catastrophic forgetting using context-dependent gating and synaptic stabilization. *Proceedings of the National Academy of Sciences*, *115*(44), 1–12. <https://doi.org/10.1073/pnas.1803839115>